MULTISPECTRAL DETECTION OF GROUND TARGETS IN HIGHLY CORRELATED BACKGROUNDS

THESIS

Jason Eric Thomas
Second Lieutenant, USAF

AFIT/GEO/ENP/94D-06

DEPARTMENT OF THE AIR FORCE
AIR UNIVERSITY
AIR FORCE INSTITUTE OF TECHNOLOGY

Wright-Patterson Air Force Base, Ohio

AFIT/GEO/ENP/94D-06

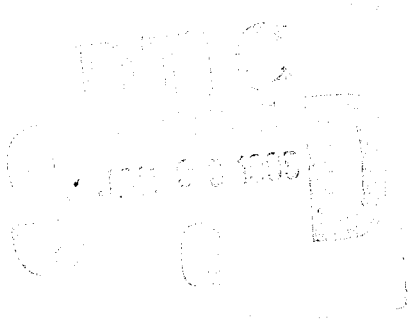

MULTISPECTRAL DETECTION OF GROUND TARGETS IN HIGHLY CORRELATED BACKGROUNDS

THESIS

Jason Eric Thomas
Second Lieutenant, USAF

AFIT/GEO/ENP/94D-06

Approved for public release; distribution unlimited

AFIT/GEO/ENP/94D-06

MULTISPECTRAL DETECTION OF GROUND TARGETS IN HIGHLY CORRELATED BACKGROUNDS

THESIS

Presented to the Faculty of the School of Engineering
of the Air Force Institute of Technology
Air University
In Partial Fulfillment of the
Requirements for the Degree of
Master of Science

Jason Eric Thomas, B.S.
Second Lieutenant, USAF

December 1994

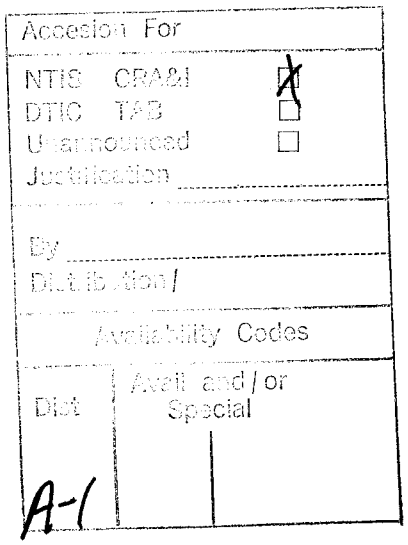

Approved for public release; distribution unlimited

Acknowledgements

I wish to thank Captain Ray O. Johnson, USAF, for the many enlightening discussions and for his support throughout this thesis work, and to thank my advisor, Dr. Theodore Luke, for his guidance and for lessons learned.

Special thanks are due to my parents, Ray and Susan, who have done more for me than any son might ask. Any success I have achieved has been because of your love and the pains you took to instill in me a sense of morality and the best of values.

Finally, most of all, I wish to thank my wonderful fiance, Suzi, who brought me cheer over a phone line and gave me motivation to persevere during the difficult days. My life will not 'begin again' after graduation, but rather in April, when I can begin it again with you. All my love is yours forever.

Jason Eric Thomas

Table of Contents

List of Figures

List of Tables

Abstract

Multispectral detection methods attempt to discriminate targets in a dominant clutter background using multiple images of the same real-world scene taken in different narrow spectral bands in the infrared. Detection is possible due to the empirically-observed phenomenon that the radiance of man-made objects, such as a tank or truck, often lies off the main spectral correlation axis of that of natural backgrounds. Radiometric measurements of several vehicles and a tree canopy background taken over three days in June, 1994 were used to examine the factors affecting multispectral detection. Results clearly showed that the processes which provide for higher spectral correlation of natural backgrounds tend to diminish the spectral separation between the background and target. Very high correlations between IR spectral bands for the targets and background were found to exist. The degree of correlation between bands in the LWIR was found to be higher than that for the MWIR for the correlation levels (ρ) of interest, $\rho \geq 0.99$. The MW/LW combinations were found to almost never produce these high correlations.

In addition, a scoring method for use in ranking pairs of spectral band pairs over multiple collection instances was developed and evaluated. The score was intended to rank combinations of spectral bands which provide consistent, if moderate, performance over bands which may provide both excellent and unacceptable signal-to-clutter ratios (SCRs) over the same observation period. The scoring method found more stable spectral pairs,

and, for data reflecting more difficult detection situations, produced rank-ordered lists of wavelength pairs which exhibited higher mean, minimum, and maximum SCRs than were produced by simply ranking the bandpairs by average SCR value.

MULTISPECTRAL DETECTION OF GROUND TARGETS IN HIGHLY CORRELATED BACKGROUNDS

I. Introduction

1.1 Motivation

The United States Air Force currently has only a limited capability to search large areas of a battlefield for hidden targets. This problem was identified during the Persian Gulf War when Iraqi mobile Scud missile launchers frequently evaded detection despite the large numbers of warplanes the United States had committed to their detection and destruction. One major new area of research which shows promise for developing an accurate and reliable wide-area search capability is that of multispectral detection methods.

Current infrared (IR) sensors detect the infrared radiation emitted by a target across relatively wide portions of the electromagnetic spectrum in either the mid- or far-IR regions, often defined to be wavelengths from approximately 3.0–5.0 microns and 8.0–12.0 microns, respectively [15, 12]. The total radiance emitted by the target within these regions is often substantially different from the total radiance of the background. When such is the case, the contrast allows the target to be distinguished from the background and displayed to the system operator who can then engage it as appropriate.

However, potential targets and backgrounds normally exhibit large variability in their respective temperatures and emissivities. Such variability can often give rise to a situation known as 'thermal crossover', an instance in which, over the portion of the IR spectrum of interest, the total radiance of the target is the same as that of the background. Under these conditions, there is no contrast between the target and background in a broadband IR sensor image, and the target is, effectively, invisible. Thermal crossover most often occurs during the hours of sunrise and sunset, but may occur, because of weather conditions and other factors, at any time of the day or night [7].

Current airborne IR sensors are used mainly for targeting and weapon delivery, and are not suited to performing the wide-area search mission. The multispectral detection methods being developed today are intended to provide this capability to the Air Force. In multispectral detection methods, multiple, relatively narrow regions of the IR spectrum are examined simultaneously to discriminate between target and background. The techniques have been used to detect targets under conditions which broadband IR sensors cannot [7]. They also show potential for providing high probabilities of detection with low false alarm rates, traits deemed essential for achieving effective automated target detection [18].

1.2 Problem

The most important problem in multispectral detection is the selection of the spectral bands which will be used to find a particular target in a particular background. Choosing the spectral bands to be examined is a form of feature selection in the sense of a classical

pattern recognition problem. Solutions to such problems begin with determining a set of features which are characteristic of the pattern signal and can be used to identify the signal's presence and/or classify its type [11]. The efforts of the Air Force's Joint Multispectral Sensor Program (JMSP) to develop multispectral detection methods are currently focused primarily on the detection problem, although the techniques may eventually demonstrate a capability to classify targets as well.

The problem studied during this work was how to select a small number of spectral band pairs which will provide for the detection of targets, using representative radiometric measurements of specific targets and natural backgrounds. The correlation of natural backgrounds and the spectral separation from these backgrounds by man-made objects are the parameters which affect multispectral detection. These were examined using the most recent JMSP radiometric data, collected in June 1994. In addition, a new method to rank-order the bandpairs using data from multiple experiments taken at different times and under different conditions was developed. This development of a new ranking priority was intended to address the question of how to best find spectral pairs which promise accurate detection for more than one type of detection situation.

1.3 Key Results

The parameters affecting current multispectral detection methods were calculated and compiled for various targets against the same natural background of trees for experimental data from the latest of four JMSP multispectral radiometric collections. The results of

this compilation confirmed that a phenomenon which had been observed in the prior data sets is evident in the fourth. Specifically, the processes which provide for higher correlation of natural backgrounds at multiple wavelengths tend to diminish the spectral separation between the background and man-made objects (such as a tank or Scud missile). Also, very high correlations between IR spectral bands for both targets and backgrounds were found to exist. The LWIR was found to exhibit high correlation between spectral bands more often than either the MWIR or MW/LWIR regions. Bandpairs which exhibited these high correlations were, in general, far more numerous than in the previous data collections.

The utility of using a scoring method to rank pairs of bands was evaluated against that of ranking the bands by the signal-to-clutter ratios (SCRs) which they exhibit. The score was intended to rank combinations of spectral bands which provide consistent, if moderate, performance over bands which may provide both excellent and unacceptable SCRs over the same observation period. The *score* was defined as

$$Score = \frac{\mu - T_b}{\sigma} \tag{1}$$

where μ is the mean SCR value over the observation times in question, σ is the standard deviation of the SCRs, and T_b is the minimum 'acceptable' SCR. The scoring method did result in the selection of more stable choices from the data, and, for the more difficult detection situations, actually produced rank ordered lists of pairs which exhibited higher average SCR than those listings which were based solely upon the SCR values.

1.4 Organization of this Thesis

This thesis is divided into five chapters. The first chapter gives some of the important considerations which have spurred the many new efforts to develop multispectral detection methods, and introduces the general concept behind them. The second chapter presents the foundations which can justify modeling infrared imagery as the result of independent random processes. The multispectral techniques being considered to detect ground targets are based upon this idea, and are also described in chapter two. The third chapter explains the methodology of this thesis work and the origin of the data used to support it. The fourth contains results and an analysis of these. Conclusions and recommendations are presented in the final chapter. Two appendices are included; the first is a directory of the experiments in each data set, and the second is a guide to using the MATLAB code written to accomplish the data analysis.

II. Current Knowledge

2.1 Some Preliminary Ideas

Most infrared sensors carried by U.S. Air Force aircraft are imaging sensors. These sensors produce a two-dimensional representation of the three-dimensional world as seen by small IR detectors through various types of imaging optics. Images captured on photographic film can be said to vary continuously in intensity across the spatial dimensions of the image field. This idea is reasonable because of the miniscule physical dimensions of each photon-sensitive molecule embedded in the film or photographic plate. In contrast, images which might be displayed on a monitor consist of a finite number of spatially separate points, or 'pixels'. The pixels of these images also assume only a finite number of values in the range between the highest and lowest found in the photographic analogue due to the digital techniques which are used to store and manipulate the data. Images with these characteristics are referred to as 'digital' images.

2.2 An Assumption of Gaussian Behavior in Imagery

A great deal of effort has been invested in examining the properties of digital imagery of real-world scenes. The statistical properties of real-world images have particular significance to those attempting to develop reliable target detection algorithms while keeping the computational load for the process to a minimum. Simplifying assumptions, when reasonable, are highly useful in that they can lead to simplified modeling, fewer computations, and therefore more timely solutions, often with minimal impact on overall performance. One

assumption often made with regard to digital imagery is that the distribution of the pixels (in intensity) is approximately Gaussian in form. However, imagery rarely has a Gaussian character [8], and, despite the utility in assuming this distribution, it is usually unrealistic to do so.

However, B. R. Hunt and T. M. Cannon showed in 1976 [5] that image intensity very often can be modeled as a two-dimensional function with a rapidly varying local spatial mean and slowly varying covariance. The intensity fluctuations about the varying spatial mean are approximately Gaussian distributed, they conclude. The local mean for a position (x, y) in an image Y is defined to be the average value of the pixels within a region W around (x, y), the size of W being a fraction of the size of the image itself (see Figure 1).

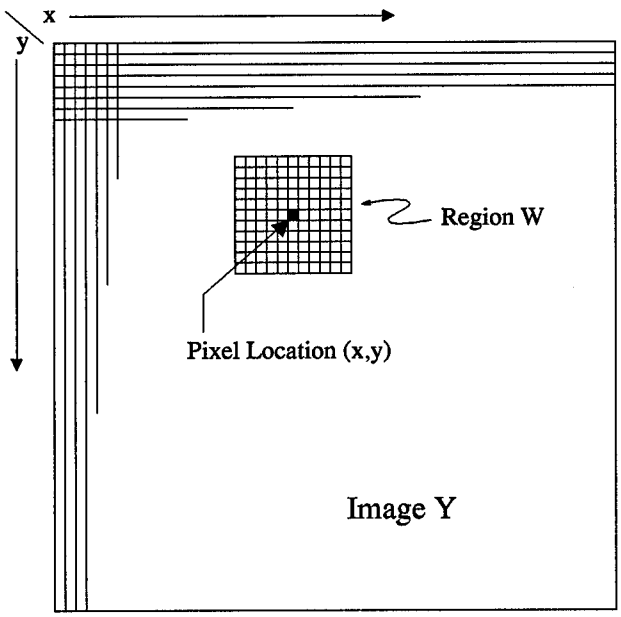

Figure 1. Use of a Spatial Mask W to Calculate Matrix of local Means

Hunt and Cannon estimated the local mean of numerous images, originally using several two-dimensional Gaussian point-spread functions with standard deviations of from 5 to tens of pixels as the mask W. They also reported achieving extremely similar results using simple square masks, and more recent papers [3, 9, 14] suggest that the local mean estimation be calculated

$$\overline{Y} = \frac{1}{N^2} \cdot [Y * W] \tag{2}$$

where ' $*$ ' denotes discrete 2-D convolution and W is a square $N \times N$ matrix of ones, with N an odd number. $\overline{Y}(x, y)$ is therefore the average of the intensities within mask W centered on (x, y), and $\overline{Y}$ is the matrix of all such means. The matrix of local means is subtracted from Y to form the processed image $\widetilde{Y} = Y - \overline{Y}$ which has a histogram that is approximately Gaussian. Selecting the most appropriate mask size from $N = 3, 5, 7, 9 \ldots$ etc., is done by choosing the size N which results in a histogram of the intensities in $\widetilde{Y}$ which has the smallest third moment, since the third moment of a Gaussian distribution is zero [3, 5, 9]. This choice has been observed to produce the most Gaussian behavior when local mean removal is performed on actual imagery, infrared and otherwise [3, 5]. The residual images which are produced by such pre-processing therefore may reasonably be modeled as having a Gaussian character, a very convenient assumption. The statistics of Gaussian distributions are well known, and being able to assume this form for the pixel intensities of these processed images can make the mathematical development of multispectral detection schemes much easier.

2.3 Covariance Between Images

Gaussian distributions of more than one dimension may be characterized fully by a mean vector and a covariance matrix. A review of some notation and mathematical concepts from statistical probability as they apply to the covariance properties of images is needed in order to set the framework for building the description of infrared imagery which is used in the multispectral detection paradigm. The following development is based upon the treatments found in [6] and [17].

To begin, if X is a random variable, let $\underline{x}$ represent an $(n \times 1)$ column vector of n observations of X:

$$\underline{x} = \begin{bmatrix} X_1 \\ X_2 \\ \vdots \\ X_n \end{bmatrix} \tag{3}$$

The transpose of the vector $\underline{x}$ has dimension $(1 \times n)$ and is designated $\underline{x}^T$, so that

$$\underline{x}^T = [X_1, X_2, \ldots, X_n] \tag{4}$$

The 'expected value' of the random variable X is the value which X would be seen to most often assume if an infinite number of observations could be made. An estimate of the expected value which is calculated using a finite number of realizations of X is familiarly known as the average, or mean, of X and is designated with the use of the *expectation operator* as $E[X]$.

If Y is another random variable, and $\underline{y}$ contains n observations of Y taken concurrently with the observations of X, the expected value of the product of the random variables X and Y is calculated by averaging the product of the observations of the two variables and is expressed $E[XY]$. If we now designate the mean of X by $m_X = E[X]$, the variance of X can be written

$$var(X) = E[(X - m_X)(X - m_X)] = E\left[(X - m_X)^2\right] = \sigma_X^2 \tag{5}$$

Similarly, the variance of Y is

$$var(Y) = E\left[(Y - m_Y)^2\right] = \sigma_Y^2 \tag{6}$$

In this discussion of expectation, no connection has been assumed between the processes which determine the values of variables X and Y. But suppose now that vectors $\underline{x}$ and $\underline{y}$ contain the intensities of the individual pixels of two images of the same real-world scene, R_1 and R_2, respectively. Image R_1 is taken at one wavelength in the MWIR, say 3.0 microns, and image R_2 is of the scene at a different wavelength, perhaps 3.7 microns. The images are co-registered, meaning that two pixels, one in R_1 and the other in R_2, which represent the same part of the real-world scene are at the same location in their respective images. The n pixel values are entered into the vectors in some way that is deterministic, and the ordering is the same for both, therefore the intensities may be thought of as corresponding observations of the two variables X and Y (which may or may not be random in this case).

X_i , where $i = 1, 2, 3, \ldots, n$, is therefore the intensity of pixel i at a wavelength of 3 microns and Y_i is the intensity of this same pixel at 3.7 microns.

The covariance matrix M between X and Y has dimension (2×2) and is formulated

$$M = \begin{bmatrix} E[(X - m_X)(X - m_X)] & E[(X - m_X)(Y - m_Y)] \\ E[(Y - m_Y)(X - m_X)] & E[(Y - m_Y)(Y - m_Y)] \end{bmatrix} = \begin{bmatrix} \sigma_X^2 & \sigma_{XY} \\ \sigma_{YX} & \sigma_Y^2 \end{bmatrix} \tag{7}$$

The off-diagonal components of M above are also sometimes written $\rho\sigma_X\sigma_Y$ where ρ is the correlation coefficient between X and Y. The correlation coefficient for these vectors is formally defined in [17] as

$$\rho = \frac{\sigma_{XY}}{\sigma_X\sigma_Y} \tag{8}$$

The correlation coefficient takes on values between minus one and one. Values near zero indicate little or no correlation between two variables, while values near one and minus one indicate high positive and negative correlation, respectively.

If we extend our consideration beyond two dimensions in order to describe the use of an arbitrary number of multiple bands, a covariance matrix calculated for J co-registered images will have dimension $(J \times J)$ and be of the form

$$M = \begin{bmatrix} \sigma_1^2 & \sigma_{12} & \cdots & \sigma_{1J} \\ \sigma_{21} & \sigma_2^2 & \cdots & \sigma_{2J} \\ \vdots & \vdots & \ddots & \vdots \\ \sigma_{J1} & \sigma_{J2} & \cdots & \sigma_J^2 \end{bmatrix} \tag{9}$$

Look again at the final notation for the covariance matrix of Equation 7. It is always true that $\sigma_{XY} = \sigma_{YX}$, and henceforth both will be written σ_{XY} for convenience. In addition, note that the square root of the variance (a scalar) is commonly called the 'standard deviation' and generally designated by the symbol σ. Therefore, with regard to a variable X, the standard deviation is represented by σ_X, the variance by σ_X^2, and the covariance of X with another variable, Y, by σ_{XY} [17].

Jiah Chen and Irving Reed have reported on the properties of the covariance matrices of co-registered images which have been pre-processed by local mean removal [3]. The two researchers calculated the covariance matrices of various sizes of sub-images of co-registered multiple-image sets which had been first processed as described in the preceding section. They found that the covariance matrices of small sub-images very often could be approximated by diagonal matrices, because the off-diagonal covariance values were often much smaller than the variances located along the main diagonals. Chen and Reed propose that this indicates the intensity fluctuations are random, or white, in the same sense as that of 'white noise'. After local mean removal, the Gaussian character of the intensity fluctuations is evident in histograms of the entire processed image. The maximum size sub-image for which the diagonal approximation remains valid, however, is typically small with respect to the main image (32×32 in the 512×512 pixel imagery examined by Chen and Reed) [3].

No assumptions concerning the independence of the image pixels from their neighbors were made by Chen and Reed. But having found a basis for the assumption of both Gaussian and random behavior in images, showing that image pixels may justly be considered

independent from one another becomes an extremely tantalizing goal. Evidence that may justify such an assumption, produced by A. Stocker, I. Reed and X. Yu, is given in Figure 2. Taken from [14], the figure shows the two-dimensional autocorrelation (normalized to have a maximum value of one) of a 256×256 infrared image of a site near Adelade, Australia which was collected by the NASA-developed Thermal Infra-red Multi-spectral Scanner (TIMS). Before the autocorrelation was computed, the image was, once again, processed to remove the space-varying local mean value, in this case with an 11×11 pixel window. The axes of Figure 2 are labelled in vertical and horizontal pixel lag which indicates how severely the two copies of the same TIMS scene were mis-registered when the correlations between the pixels in the first and those in the second were calculated. The contours show constant values of the normalized autocorrelation as the two images are shifted in two dimensions. As expected, the maximum value is at coordinates $(0, 0)$, demonstrating that the maximum correlation between the image and a copy of itself occurs when they are co-registered. As seen in the figure, when one copy is offset from the other by a small amount, the overall correlation between the pixels in copy one and copy two begins to decrease rapidly. When the images are subjected to a shift of one pixel, the autocorrelation is approximately one-fifth that of the maximum value. The value drops near zero and remains there for any greater degree of shift. The pixels of the processed TIMS image are nearly decorrelated, even from their immediate neighbors [14]. The mathematics of statistics and probability show that the correlation between two independent random variables is zero. Stocker, Reed and Yu therefore

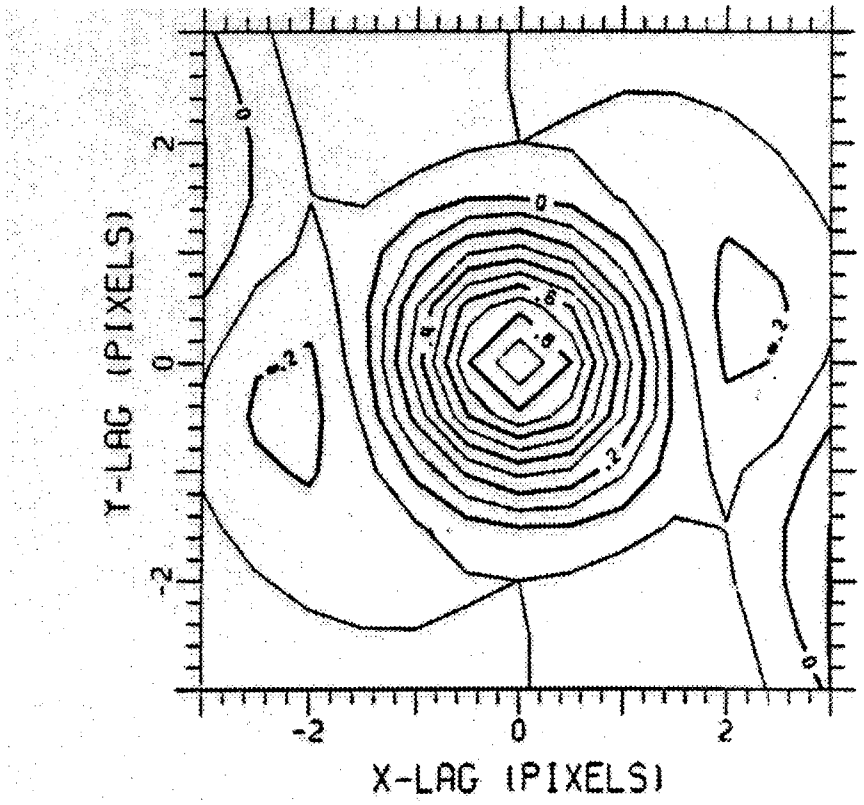

Figure 2. 2-D Autocorrelation of Pre-processed TIMS Image Suggesting Pixel-to-Pixel Independence

suggest that it is reasonable to treat the pixel intensity fluctuations of infrared images as if each is independent from every other [14].

If this last statement is accepted, then the J-dimensional clustering of the pixel values in a small sub-region from J pre-processed image frames can be characterized as one or more multivariate Gaussian distributions of independent random events. Being able to model infrared imagery as the result of independent random events makes the many powerful tools of statistical probability available for use in formulating multispectral detection algorithms.

2.4 *Correlation Between Images of Natural Backgrounds*

Experiments have shown that the infrared images of natural backgrounds are often highly correlated between narrow spectral bands of the mid-wave IR (MWIR) and far- or long-wave IR (LWIR) spectrum [1]. Figure 3 shows a scatterplot of intensities for four different pairs of wavelengths, two in the MWIR and two in the LWIR, for 70 measurements of coniferous trees. The data come from one experiment of a recent collection of radiometric

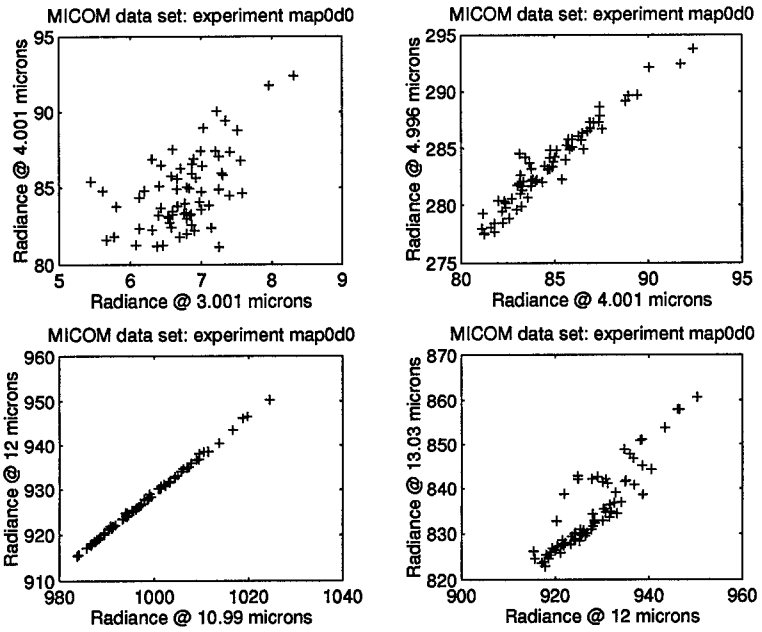

Figure 3. Correlations of 70 Radiometric Measurements of Tree Canopy for Several Pairs of IR Spectral Bands

measurements which is described and discussed in chapter three. The measurements in the figure were taken at 10:32, the morning of 20 July 1993, at the U.S. Army's Redstone Arsenal in Hunstville, Alabama, and have units of $\mu W/(cm^2 \cdot Steradian \cdot \mu m)$ [1]. A high degree of correlation between the wavelengths of 11 and 12 microns is clearly evident, as are varied lower degrees for the three other pairings. The sample points plotted in Figure 3

correspond to separate portions of the tree canopy. However, these particular data were not produced by an imaging instrument, but taken individually over the span of several minutes. Sets of real infrared images have been shown to demonstrate similar degrees of correlation between their respective pixel intensities, and the correlation is preserved in images subjected to local mean removal [18]. The data in Figure 3 can therefore be thought of as representing the light intensity, at the respective wavelengths, of individual pixels which might be present in a pre-processed infrared image of the trees. The scatterplot contains no spatial information to indicate what portion of the image each point might represent. It merely shows the correlation, from one pixel to another, between each rise and fall of the radiance levels across the trees at the paired wavelengths. Note that this is different from the concept of correlation between neighboring pixels in each individual image, which was discussed previously. The correlations demonstrated in Figure 3 are spectral, not spatial. The intensity of one pixel at 12 microns may be linked to the pixel intensity at 11 microns, thereby demonstrating spectral correlation. However, spatial independence between pixels is still assumed, meaning that, for all wavelengths, the intensity of any pixel in the image is independent from that of any other pixel. Multispectral detection of a target within an image, such as a truck in trees or scrub bushes, is based upon the observed phenomenon that the band-to-band correlations of pixels from man-made objects often lie off the main axis of the distribution of the background pixels. Figure 4 depicts a hypothetical example of how the pixels of an infrared image containing a target against a natural background might be distributed in a two dimensional scatterplot of intensities at a pair of narrow spectral bins

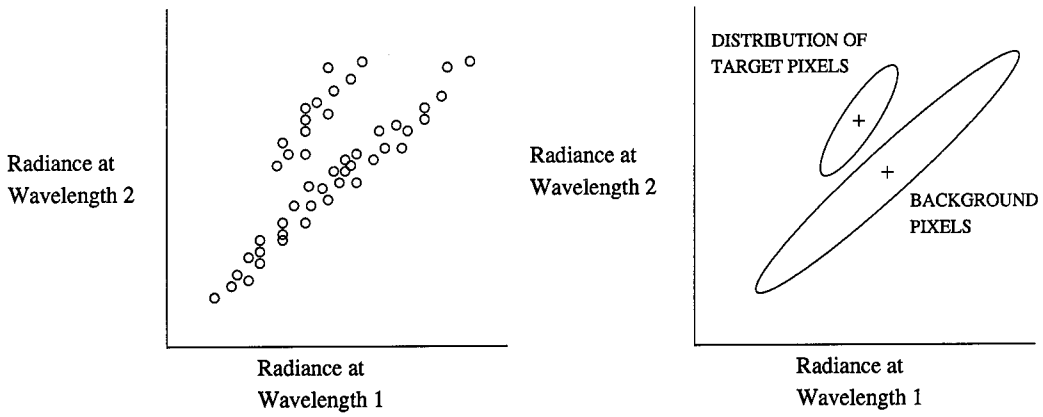

Figure 4. Hypothetical Depiction of Spectral Separation for a Target and Background

centered at different wavelengths. The target distribution is sometimes referred to as having 'color' [14, 18] with respect to the background due to the evident separation between the means of the distributions in 2-D wavelength space. Spectral separation and color separation are terms which are used interchangeably to refer to this property [7].

Now assume for a moment that the spectral mean radiance of a target with respect to the mean of a background were as depicted in Figure 5 over some portion of the IR spectrum. The hypothetical detection situation of Figure 4 above might be produced by scatterplotting the pixel intensities at the wavelengths indicated in Figure 5. The spectral separation results from the fact that mean target radiance is lower than the mean background radiance in wavelength #1, while the opposite is true at wavelength #2. Many different factors can lead to this circumstance. Differences in temperature between target and background can cause spectral separation. Another common cause is the difference in spectral emissivities of the target and background at the two wavelengths. The situation in Figure 4 would be a good one for detection because the target distribution is well-removed from the back-

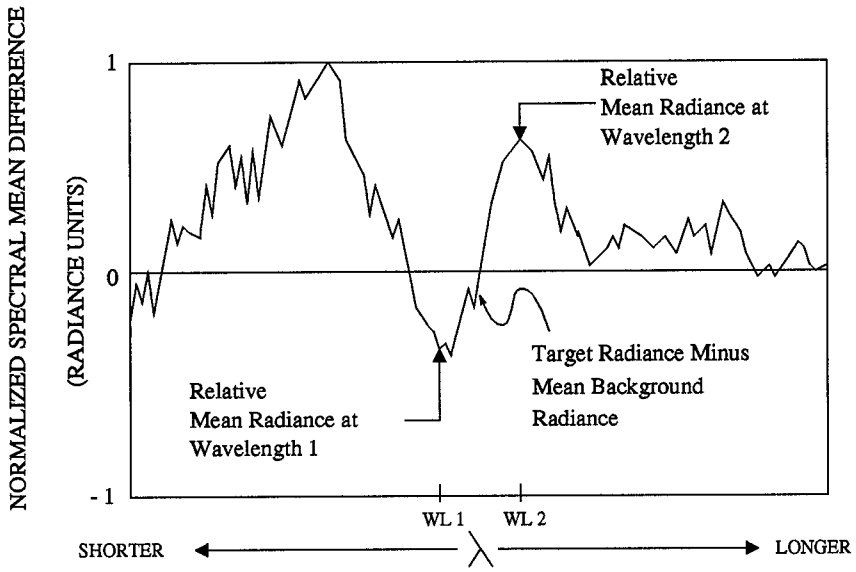

Figure 5. Normalized Radiance Difference Between Hypothetical Target and Background of Figure 4

ground distribution. This spectral separation in multiple-wavelength space is fundamental to multispectral detection of targets in correlated backgrounds. The 'coloring' of man-made objects with respect to natural backgrounds has been observed often enough to encourage the development of techniques to exploit this behavior [4, 18].

2.5 Methods for Detection

Target detection may be attempted under two conditions; when one or more targets are actually present in an image, and when no target is present. A system is said to attempt detection under the H_0 hypothesis when no target is present, and to attempt detection under hypothesis H_1 when a target is present. Any target detection which is made under

hypothesis H_0 is a false alarm. With the paradigm established for multispectral detection in the previous section, under H_1, a detection may be either a false alarm or a true detection. For instance, a tree pixel might still be classified as a target by the detection system while properly classifying an image pixel from a tank as a target as well. There is also a chance under H_1 that the system may not recognize the existence of the target at all, resulting in a missed detection [10].

Three basic techniques for processing multispectral data are the minimum clutter processor, the spectral matched filter, and the 'RX' algorithm. These three techniques are described in [15], and can all be derived from a generalized linear multidimensional filter. These three methods have been the primary methods proposed for multispectral detection for a number of years, and were the basis for the work described in this thesis. The discussions of each method below are based upon the work in [14],[15], and [18].

Consider J co-registered sub-frames, each from an image taken in a different IR spectral band and pre-processed by local mean removal. The total number of pixels in each frame is n. Let $\underline{x}_1, \underline{x}_2, \ldots, \underline{x}_n$ be column vectors containing the intensities in the J sub-frames for each of the n pixels. Each $\underline{x}$ is therefore a $(J \times 1)$ multispectral vector for one pixel in the input image. A $(J \times n)$ matrix X of these n multispectral observations may be formulated

$$X = \left[\begin{array}{cccc} \underline{x}_1 & \underline{x}_2 & \underline{x}_3 & \cdots & \underline{x}_n \end{array} \right] \tag{10}$$

A J-dimensional linear filter will modify the input observations in X through matrix multiplication with a $(J \times 1)$ weight vector $\underline{w}$. The output $\underline{y}$ of such a filter is given by [10, 15]:

$$\underline{y}^T = \underline{w}^T X \tag{11}$$

A spatial filter $\underline{s}$ of dimension $(n \times 1)$ is often multiplied with $\underline{y}$ to produce a scalar output,

$$y = \underline{w}^T X \underline{s} \tag{12}$$

The use of a spatial filter is based upon a presumption that the size and shape of a target in the image may be known beforehand, and that the target in the image will consist of more than one pixel [14, 15]. The spatial filter therefore places an additional constraint on the system by requiring that pixels which are spectrally separate from the background clutter in wavelength space form a contiguous region in the image itself before the filter will produce a substantial output. When the spatial filter mask is centered on a region of many pixels which are spectrally separate from the background, the scalar output is expected to be above some threshold for deciding if a target is indeed present. When sub-pixel target detection is attempted, the spatial filter is not needed and the pixels from the sub-frame from the pre-processed image are evaluated individually, rather than collectively, against the threshold to achieve target detection. In either case, if the output of the filter is greater than this threshold, the single pixel or group of pixels in the image is classified as a target.

Signal detection is almost invariably performed amid some form of noise, loosely defined to be any process which can obscure or eliminate the pattern one seeks to detect [10, 11].

The parameter which is frequently used to evaluate the effect of system noise on the output is the signal-to-noise ratio (SNR). SNR is defined to be the expected value of the signal divided by the standard deviation of the system noise [12]. The task of detecting a target in the midst of tress or brush in an image is one of recognizing the target signal hidden within the natural background. The pixels from the background can be thought of as noise, but this noise is not internal to the detection system, and therefore is usually termed 'clutter'. The measure of target detectability in images is termed the signal-to-clutter ratio, or SCR. From the above discussion, the general expression for the SCR for the linear spectral filter (with a spatial filter) described by Equation 12 is [15]

$$SCR = \left[\frac{E^2[y] \ under \ H_1}{var(y) \ under \ H_0} \right]^{\frac{1}{2}} \tag{13}$$

Figure 6 shows three vectors $\underline{b}_{1,2,3}$ with respect to a background clutter distribution of high correlation for an image for which J=2 bands. As considered in [14] and [15], a vector $\underline{b}$ represents a single pixel of the image. The relative position of $\underline{b}$ with respect to the center of the clutter is the characteristic used to decide if $\underline{b}$ represents a target pixel or a pixel of the background. The center of the background clutter is located at the origin when modeling the image sub-frame since the histogram of an image subjected to local mean removal pre-processing has an approximately Gaussian histogram with a mean value of zero [14]. The Figure also shows the relationships of the hypothetical spectral radiances which might position each target $\underline{b}$ vector relative to the mean radiance of the background. The vertical axis is normalized by the maximum difference in the radiance levels between target

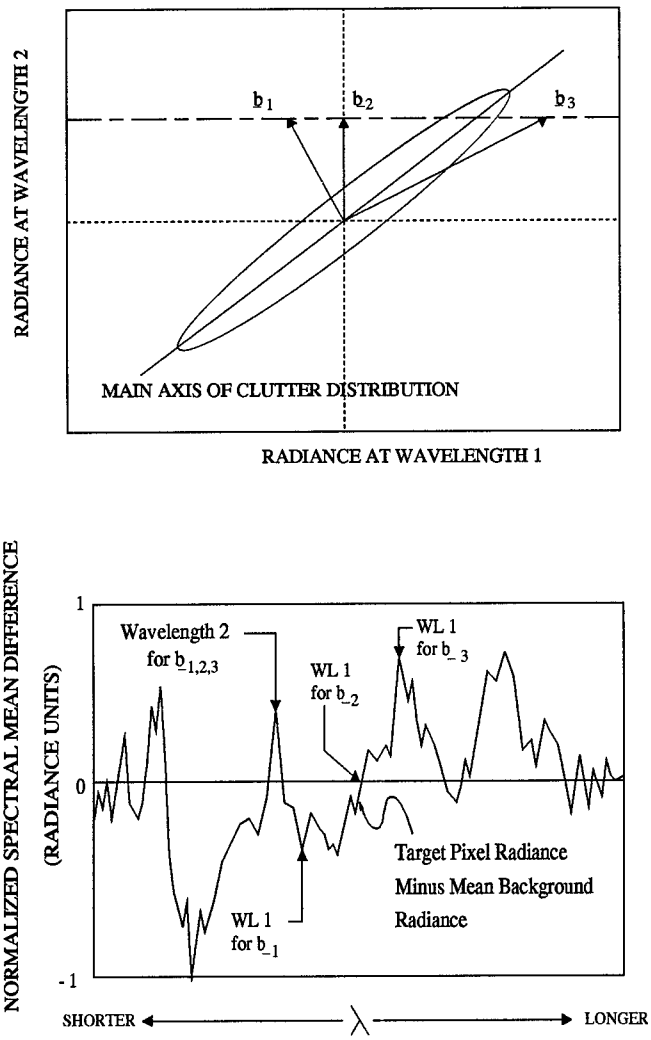

Figure 6. Relation Between Signal Vectors and Background Mean for Three Bandpairs

and background over the portion of the IR spectrum of interest. This positioning of $\underline{b}$ due to the relative radiance levels in each band has been described in terms of differing spectral apparent temperature as well. The radiance levels are converted to apparent temperature by assuming a common emissivity for both target and background, then calculating the 'apparent' temperature of each based upon the measured radiance from both over the IR spectrum [13].

The three detection filtering techniques outlined in [15] are obtained by selecting three different spectral weight vectors, $\underline{w}$, but in general, the performance of each depends upon the signal-to-clutter ratio of the scalar detector output of Equation 12. Given the above discussion of the target vector $\underline{b}$, the SCR may be written [15]

$$SCR = \left[\frac{E^2\,[y]\ under\ H_1}{var(y)\ under\ H_0}\right]^{\frac{1}{2}} = \left[\frac{(\underline{w}^T\underline{b})^2}{\underline{w}^T M \underline{w}}\right]^{\frac{1}{2}} \tag{14}$$

The following sections describe the choices of the weight vector $\underline{w}$ which give rise to the three methods for detecting a target vector $\underline{b}$ which is spectrally separate from a background distribution.

2.5.1 The Minimum Clutter Processor. The Minimum Clutter (MC) processor performs 'weighted band differencing' of the image vectors in J-bands and is used to minimize the total power of the background clutter [15]. The process is illustrated in Figure 7 for the dual-band case (J=2). If the background pixel intensities for two bands are highly correlated, plotting the image intensities will give two traces which are very similar to one another within some scale factor, as shown in Figure 7a. If the means are subtracted from each trace and one is scaled with respect to, and then subtracted from, the other, target pixels which lie off the main axis of correlation will produce a larger residual value (Figure 7d). Thresholding the residual vector will identify vector elements which are not well correlated with the majority of the pixels. These residuals are expected to be pixels from the target, provided the target is colored with respect to the background. A spectral weight which accomplishes this scaling and differencing is

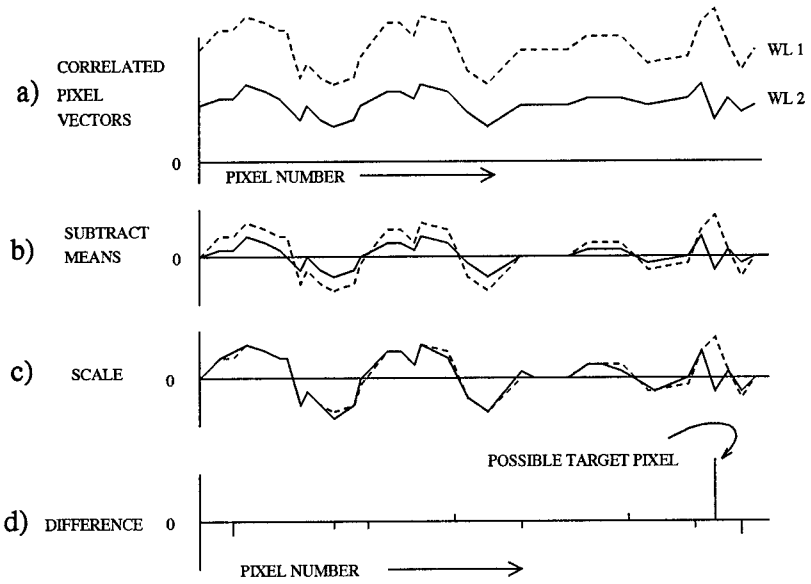

Figure 7. Illustration of Weighted Band Differencing

$$\underline{w}_{MC} = \begin{bmatrix} 1 \\ \\ -\rho \cdot \sigma_1/\sigma_2 \end{bmatrix} \tag{15}$$

and has been found to be the weight which minimizes the magnitude of the background residual intensity values, as required for the MC processing [15, 16].

2.5.2 The Matched Spectral Filter. The matched filter, like the MC processor, takes advantage of the difference in the means of the target and background distributions, a situation like that shown previously in Figure 4. Whereas the MC processing minimizes the total squared summed magnitude of the background, matched filtering maximizes the signal-to-clutter ratio (SCR) of an expected target signal with respect to the background clutter. In general, the J-dimensional weight vector associated with the matched filter for a

known $(J \times 1)$ target vector $\underline{b}$ and known $(J \times J)$ spectral covariance matrix M is [15]

$$\underline{w}_{MF}^{T} = \underline{b}^{T} M^{-1} \tag{16}$$

The covariance matrix M for J=2 bands is

$$M = \begin{bmatrix} {\sigma_1}^2 & \rho\sigma_1\sigma_2 \\ \rho\sigma_1\sigma_2 & {\sigma_2}^2 \end{bmatrix} \tag{17}$$

and the SCR for the matched filter (also for J=2 bands), based upon Equation 14 may be written [14]

$$SCR = \left[(1-\rho^2)^{-1}((b_1/\sigma_1)^2 - 2\rho(b_1/\sigma_1)(b_2/\sigma_2) + (b_2/\sigma_2)^2)\right]^{\frac{1}{2}} \tag{18}$$

The improvement in the SCR which is achieved by examining a pair of bands instead of a single band is the dual-band SCR expression, given in the equation above, divided by the magnitude of the best single-band SCR (remember that negative single-band SCRs are possible, in this formulation, due to the convention used in describing $\underline{b}$). The expression for the improvement in SCR has been termed the multispectral gain, G [14, 18]. If the best single-band SCR is assumed to be associated with the center wavelength of the first spectral bin and designated SCR_1, then G can be expressed [14]

$$G = SCR/SCR_1 = \left[(1-\rho^2)^{-1}(1 - 2\rho R + R^2)\right]^{\frac{1}{2}} \tag{19}$$

where R is the ratio of the signed single-band SCRs and ρ is the correlation coefficient of the background clutter distribution in the 2D wavelength feature space, calculated as in Equation 8. R is expressed mathematically, as

$$R = \frac{(b_2/\sigma_2)}{(b_1/\sigma_1)} \tag{20}$$

As was mentioned above, the absolute value of (b_1/σ_1) is assumed to be greater than the absolute value of (b_2/σ_2) so that R takes on values between 1 and -1. The color ratio R gives a measure of the spectral separation between the target vector and the background clutter, and is called the 'color coefficient'. R has an angular dependence with respect to the background mean in the dual-band wavelength space. This characteristic is illustrated in Figure 8. Pixels aligned with the main correlation axis of the correlated clutter have color ratios of one, while pixels which are orthogonal to this main axis have a value of negative one. Lower R values indicate greater color, or spectral separation, [14], between target and background. Negative R values indicate the greatest color between target and background and are most desired. The advantage in using pairs of spectral bands increases as the background distribution becomes more highly correlated and the color ratio R decreases. This fact can be seen in the plot of the multispectral gain, G, versus the color coefficient, R, for several background correlation values in Figure 9, reproduced from [14]. The parameter G has a direct dependence upon the value of R. The dependence of the dual-band SCR upon R is not as immediately apparent, but is similar to the dependence seen in G. That is, the SCR generally increases as R decreases and becomes negative.

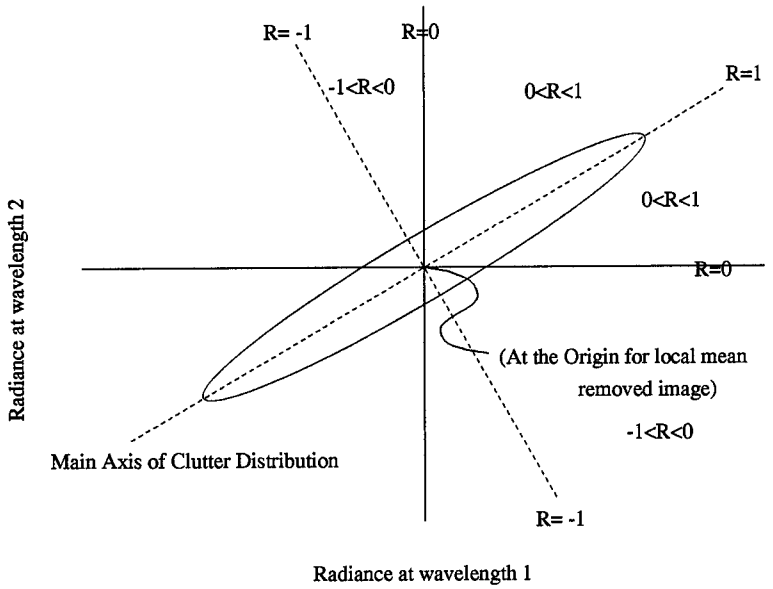

Figure 8. The Values of the Color Ratio R with Respect to the Background Distribution for Potential Targets in the 2D Wavelength Feature Space of the Multispectral Detection Paradigm

2.5.3 The 'RX' Filter. A problem with the matched filter is the requirement to assume that both the target vector and the covariance matrix of the background may be known exactly. This is an unrealistic expectation. The RX algorithm, so-named due to the notation used for its derivation in [14], implements an adaptive filter which explicitly substitutes estimates of the target vector $\underline{b}$ and the covariance matrix M into the weight vector associated with the matched filter (Equation 16). These are maximum likelihood estimations [18] which are based upon the observed image data and the assumption of a multivariate Gaussian form for the background distribution. Because these estimates are used, the algorithm is considered to be an approximation to the matched filter. The weight for the RX algorithm is

$$\underline{w}_{RX}^{T} = \hat{\underline{b}}^{T} \hat{M}^{-1} \tag{21}$$

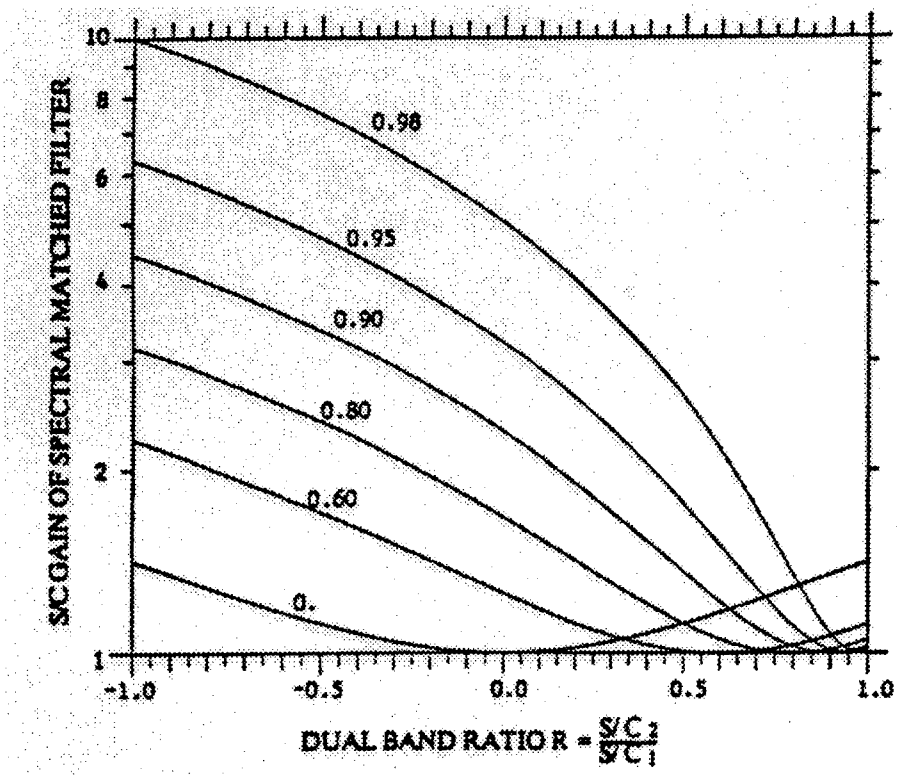

Figure 9. Multispectral gain (G) versus the color coefficient R

The target vector estimate, $\hat{\underline{b}}$ is

$$\hat{\underline{b}} = \sum_{i=1}^{n} \underline{x}_i s_i = X\underline{s} \tag{22}$$

where the spectral observation matrix X and the spatial filter $\underline{s}$ are the same as previously defined. The true covariance is estimated by calculating the covariance matrix $\hat{M}$ from the number of pixels present in the pre-processed sub-frame:

$$\hat{M} = \frac{1}{n}\sum_{i=1}^{n} \underline{x}_i \underline{x}_i{}^T = \frac{1}{n} XX^T \tag{23}$$

This result is the average (or expected value) of XX^T, and for J=2 bands is the same result as that of Equation 7. This covariance matrix calculation would be the exact covariance

matrix of the background clutter if there were an infinite number of pixels available from which to form the estimate. The RX algorithm incurs a loss in sensitivity with respect to the perfectly matched filter, but this loss may be limited to about 1 dB of SCR if the number of independent pixel observations used to calculate $\hat{M}$ is sufficiently large [15, 18].

The three detection methods described in this chapter are the favored candidates for performing multispectral detection. The value of the SCR in Equation 18, upon which the performance of the matched filter depends, is a function of the parameters which affect multispectral detection, namely ρ and R. Since the matched filter is usually considered to be an optimal detection method for finding the location of a known signal in high noise or clutter [14], Equation 18 provides an upper bound on the SCR that can be expected to be found under operational conditions. In addressing the fundamental question of multispectral detection (what bands provide the best target/background discrimination), dual-band SCR becomes a useful and easily interpreted measure of the potential of a given spectral band pairing to provide this discrimination. For this reason, dual-band SCR has become the metric of choice for use in examining bandpair performance, and was adopted for this thesis work as well.

III. Methodology

3.1 The JMSP data collections

To date, the JMSP has completed the four radiometric data collections listed in Table 1. More detailed listings, which give the names and dates of all the experiments contained in each collection, are provided in Appendix A. Brief descriptions of the targets and backgrounds measured during each collection are also included.

Table 1. JMSP Radiometric Data Collections

Collection Name	Dates	Location	Description
wsmr	6–12 Jan 1993	White Sands Missile Range, New Mexico	Tanks, trucks, painted panels, desert scrub, soil, grass, mixed backgrounds
micom	14 July–6 Sep 1993	Redstone Arsenal Huntsville, Alabama	Military vehicles (some under camouflage nets), civilian vehicles, painted test panels, soil, coniferous and mixed tree backgrounds
wright_lab	24 Sep–29 Nov 1993	Wright-Patterson AFB, Ohio	M35 truck, painted panels, grass and soil backgrounds
symptom_slew	6–10 June 1994	Wright-Patterson AFB, Ohio	Scud B missile, Scud launch vehicle, M60 tank, M35 truck, M752 Lance missile launcher, panels, target decoys, U-Haul, tree and grass backgrounds

The instrument currently used for the data collections is a BOMEM Fourier Transform Spectrometer (FTS), specially designed to take radiometric measurements in the field [2], and is discussed in detail in the following section. The MB-100 FTS was configured to have a maximum instantaneous field of view (IFOV) of 5 milliradians, and is the sensor used to collect the radiometric measurements of the coniferous trees presented previously in Figure 3.

In general, the measurements of the targets and backgrounds in the data is one-half IFOV oversampled, meaning that half of the IFOV during each measurement overlaps that of the previous measurement. Because each measurement is taken individually, the data collected by the FTS may be treated as independent samples of the respective targets in each collection [1]. The instrument is thus suited to investigating the properties of targets and backgrounds which might someday be examined in combat scenarios by imaging multispectral IR sensors.

3.2 The Bomem MB-100 Fourier Transform Spectrometer

Reference [2] is the final report on the design and noise characterization of the Bomem MB-100 FTS. The heart of the MB-100 is a Michelson interferometer consisting of a KBr beamsplitter positioned between two cube corner retro-reflectors which are mounted on a forked scan arm as shown in Figure 10 (reproduced from [2]). The design has two complementary inputs and outputs. The first input is directed toward the target of interest and the second toward a stable cold reference, liquid nitrogen, for temperature calibration. Both outputs are sent to the two detectors, an InSb detector for the MWIR of the spectrum and a HgCdTe detector for the LWIR region. As the scan arm in the MB-100 pivots, the optical path difference introduced between the arms produces an interferogram. Sampling of this interferogram is done with reference to the lasing wavelength of a HeNe laser, which propagates through the interferometer and is used for calibration of the sample points. The sampled interferogram is then Fourier transformed to produce the target spectrum. Two interferograms are actually produced (one per detector), and the Fourier transforms are computed in real time by two digital signal processor boards and remotely linked to the control computer

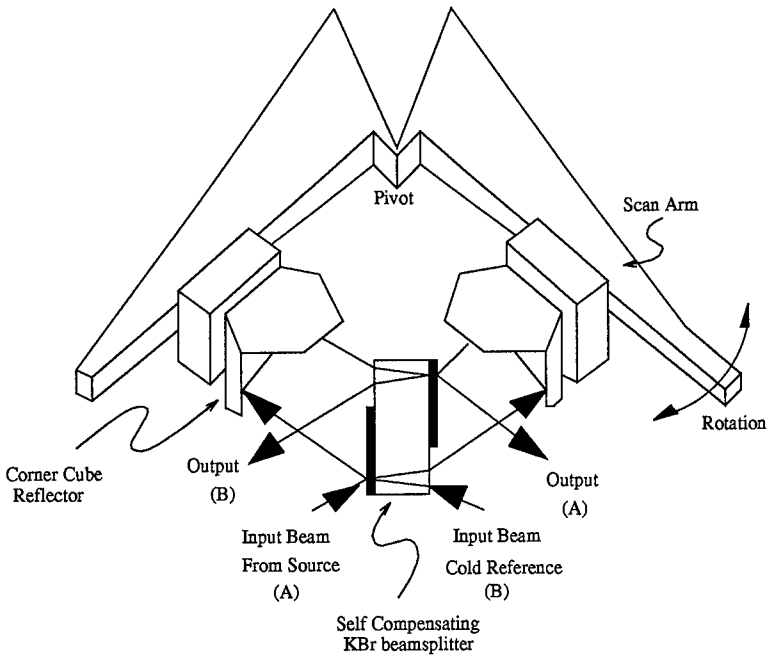

Figure 10. BOMEM MB-100 FTS Scan Arm Configuration

through a pair of RS422 interfaces. A 10-inch Cassegrain telescope and collimator assembly serve as the input optics for the FTS, and the system has an instantaneous field-of-view of 5 milliradians with the limiting apertures fully opened. A dichroic beamsplitter is used in the collimating assembly to direct part of the input to a CCD camera which can then be used to boresight the FTS through the common telescope aperture. The entire assembly is set on a motorized mount, and azimuth and elevation are input to the mount by the control software. The experiments are thus completely automated, once programmed, and a typical collection of fifty samples of various targets and backgrounds may take from approximately 8–15 minutes [1]. Pointing repeatability is determined by the backlash and run-out of the rotary stage gearing mechanism. For uni-directional scans the repeatability is better than 50

microradians, or 0.01 times the maximum IFOV of 5 milliradians. for bi-directional scans, the repeatability is 0.03 $\times$ maximum IFOV [2].

FTS radiometric calibration is accomplished with the use of two Electro-Optical Industries model T1812D blackbody sources. They each provide temperature ranges from 0 to 50.0 degrees C over 12 in. x 12 in. emitter surfaces. The Environmental Research Institute of Michigan has determined that these sources maintain their temperature to within 0.15 degrees C. The temperatures of the sources are set to the anticipated range of the target scene and the sources are used to perform a two-point radiometric calibration of the FTS system just before and just after each series of radiance collections [1].

The final conclusions drawn from the noise characterization of the MB-100 FTS published in [2] are :

1) The correlation and mean difference measurements made within a single calibration cycle will be practically unaffected by anticipated miscallibrations.

2) The correlation and mean difference measurements between multiple calibration cycles are more affected [by such miscallibrations], but errors can be minimized using stable sources.

3) Expected mean difference uncertainties will be on the order of 1% apparent emissivity or less between calibration cycles.

4) Expected decorrelation due to calibration source instability will range from 0.97 to 0.999 depending on scene radiance variance [between calibration cycles].

As the analysis in [2] shows, the effects of noise on the correlations evident in the data are negligible. Therefore, sensor noise was not considered in this work.

3.3 The Statistics of the Spectral Bands

Multispectral detection seeks to exploit the frequent high correlations between spectral bands which have been observed. The techniques also require some amount of spectral separation between target and background. A few moments of reflection on these requirements quickly brings a number of questions to mind: How often do targets exhibit color relative to a particular natural background? Are there many wavelengths which produce this behavior, or only a few? Which wavelengths are they, and can favorable performance be expected a good deal of the time when choosing them?

These are not the only questions that need to be answered, but just these few suggest that an examination of the statistics of the various data sets is necessary. The *micom* and *wsmr* collections have been analyzed, and the *wright_lab* data set is currently being examined. Some trends in the parameters of interest, namely target color and background correlation, have been identified thus far, and many of them are discussed in [13]. One trend evident in the data is that natural backgrounds usually exhibit higher correlations between spectral bands in the LWIR than in the MWIR, and correlations of MW/LW bands are typically very poor [13]. Although the LWIR tends to show greater correlations, the MWIR seems to reflect greater color between man-made targets and natural background. MW/LW pairs often show the most spectral separation, but the correlations are invariably too low to be

considered for use [7, 13]. The minimum spectral correlation which is widely considered to be worthy of interest is $\rho = 0.99$ [7].

The total amount of data contained in the four collections is vast. The scope of this thesis was therefore limited to consideration of the fourth, most recent data collection. The *symptom_slew* data set was chosen over the others for two reasons. First, this collection had not been examined in any way, and yet was available soon after the start of this thesis work. Second, the majority of the experiments contain data from both targets and backgrounds taken almost simultaneously. In addition to containing target measurements which were taken concurrently with background measurements, the *symptom_slew* experiments were performed at very nearly the same times over several days, allowing a direct comparison of the detection conditions from one day to the next.

3.4 Development of a Score for Selecting Band Pairs

The JMSP data collections provide many opportunities to examine the coloring of targets with respect to natural backgrounds. Each experiment where a background and target are chosen and then examined provides an opportunity for detection. The collections contain hyperspectral data, radiometric measurements in several hundred spectral bands. The number of band combinations which might be examined by a *multi*spectral sensor is in the tens of bands, however. Therefore, one important task in developing an affordable operational multispectral sensor is narrowing consideration to a smaller number of bands. Finding a small number of bandpairs (from the many thousand combinations) which provide

for good target discrimination a majority of the time could allow for designing a sensor with a number of filter wheels to block all bands but those of interest. Such wheels serve as a mount for several narrow-band IR filters which can be rapidly rotated into position in front of an IR sensor to exclude all bands but that which the filter is designed to pass. This option is attractive because of its simplicity and the inherent savings associated with reduced complexity in an operational system [7].

A detailed examination of these opportunities is the current focus of the JMSP. One matter which is unresolved is how this data might be used most effectively to identify a small number of bands which demonstrate favorable detection conditions over varied conditions. This is of concern since factors such as weather and temperature can change substantially with time of day and the time of year.

One straightforward method of evaluating the performance of a particular set of bands over multiple experiments is to simply average the dual-band SCRs of the individual detection opportunities and choose the J bandpairs which have the highest overall SCR. This is an obvious and conceptually simple method, and it is natural that this might be the method employed to rank order a set of promising bandpairs. However, a potentially more useful method for ranking the performance of the candidate pairs is to score them based upon a set of criteria which represent a particular notion of ideal performance. For example, consider a band pair that remains above some set lower bound on SCR for every instance under consideration. A pair which did this might be a better choice than another which has very high SCR for some times of the day, but exhibits undesirably low SCRs at other times. The

mean SCR value across the day may be higher for the second pair than for the first, and yet the first pair may actually be the more desirable choice. To promote band pairs which reflect this attribute above others which may not when the mean SCRs are comparable, the following score is proposed:

$$Score = \frac{\mu - T_b}{\sigma} \tag{24}$$

where μ is the mean SCR value, σ is the standard deviation of the SCRs under consideration, and T_b is the minimum 'acceptable' SCR.

The dual-band SCR has been established as a good metric for evaluating the detection potential of a single detection opportunity. Knowledge of how often any particular pair provides the desired high SCRs may be gained if these SCR values are calculated and considered over a number of instances during a day or perhaps over a period of days. Figure 11 shows how a set of SCR's is scored in relation to the lower bound T_b. If it may be assumed that the processes which determine these SCRs influence their distribution about a mean value in some deterministic fashion, the distributions of an infinite number of such calculated SCRs over an infinite number of detection opportunities will be of the same form. Making such an assumption may or may not be justified at this point, but it may prove useful to view the SCR as a variable whose value in time is randomly distributed over some finite numerical range. In the figure, the familiar Gaussian shape is used only to illustrate the idea behind the *score* in Equation 24. No specific form for the distribution of the SCRs has been assumed, nor is it suggested that the Gaussian form is best suited to describe the SCR distribution. Figure 11 demonstrates that the value of the *score* is directly proportional to the fraction

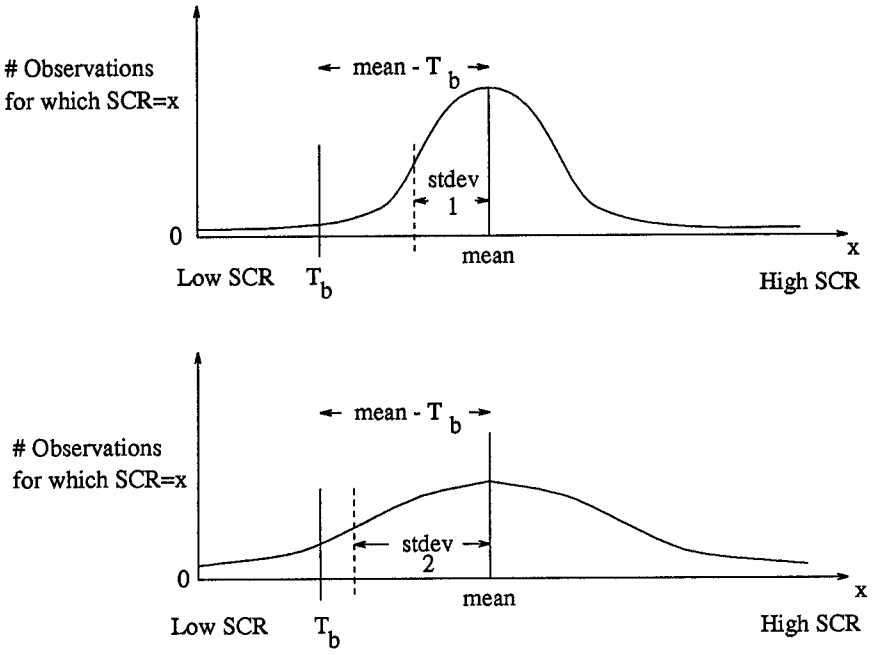

Figure 11. Scoring two SCR Distributions with Different Standard Deviations

of the total area under the distribution which is above T_b. The Figure therefore suggests that the higher the *score* for a particular pair of bands, when considered over some period of time, the more often the pair should produce signal-to-clutter ratios which are above the lower bound T_b. The second part of this thesis is devoted to determining if ranking the bandpairs by the *score* in Equation 24 exhibits any potential advantages over ranking them by average SCR value.

IV. Presentation and Analysis of Results

The three experiment series from the *symptom_slew* data set which were examined in this thesis are listed below in Table 2. The targets contained in each series are given in Table 3.

Table 2. The Data Series Examined

Experiment Name	date	time
d06nz1	06 June 1994	3:23 AM
d06nz2		5:28 AM
d06nz3		7:21 AM
d06nz4		9:10 AM
d06nz5		11:03 AM
d07nz1	07 June 1994	3:23 AM
d07nz2		5:21 AM
d07nz3		7:18 AM
d07nz4		9:09 AM
d07nz5		11:05 AM
d08nz1	08 June 1994	5:15 AM
d08nz2		7:06 AM
d08nz3		9:26 AM
d08nz4		11:14 AM
d08nz5		1:16 PM

Target and background data were collected simultaneously for these experiments. They are therefore ideally suited to examining the parameters affecting the performance of multi-spectral detectors, since the color coefficient R has meaning only with respect to a background clutter distribution. However, if one were to attempt to examine all the different combina-

tions of the spectral bands available in the data, it would entail performing $(728^2 - 728)/2$, or $264,628$ calculations each of R, ρ, SCR or whichever parameter or metric was needed. To reduce the required computations, only spectral bins at wavelength intervals of 0.1 μm from 3.0 to 14.2 μm were considered for any target or background. This binning reduced the dimensionality of the spectral matrices to (113×113), a more tractable amount of data. The width of the spectral bins was chosen to be 100 nm. JMSP researchers have generally agreed that this bin width is the smallest which may reasonably be considered for use in a multispectral sensor due to the limited dwell time available to an airborne sensor [7]. Spectral filters passing bands of smaller width than 100 nm may not admit enough photons in the time available to allow the detector to operate in the MWIR. In addition, Multispectral detection performance (evaluated through use of the dual-band SCR expression of a matched filter and Multispectral Gain G) has been observed to remain fairly constant as binning is increased to 200 nm, but to steadily drop as the width is increased beyond this point [13]. For this reason, 100 nm bin widths have been used in all investigations using the JMSP data. To allow direct comparison of this work, the choice was made to use a bin width of 100 nm for this thesis as well.

The interval of 0.1 microns between the centers of the bands is approximate because the data reflects constant sampling at intervals of wavenumber not wavelength. The data extraction process steps through values from 3 to 14.2 μm in increments of 0.1, and calculates and index into the data vector which contains the radiance values of the closest wavelength actually present in the experiment. These radiance values are then read and properly labeled

Table 3. The Targets in the Experiments

Experiment Series	Targets
d06nz_	
06 June 1994	M752_Launcher 0 11
	MAZ543_TEL 12 27
	MAZ543_Decoy 28 4
	M50_Tank 44 55
	M35_Truck 56 67
	Tree_Canopy 68 85
d07nz_	
07 June 1994	M752_Launcher 0 11
	Lance_Missile 12 14
	MAZ543_TEL 15 30
	Scud_B_Missile 31 34
	MAZ543_Decoy 35 50
	M50_Tank 55 66
	M35_Truck 67 78
	UHaul_Truck 79 8
	Tree_Canopy 82 99
d08nz_	
08 June 1994	M752_Launcher 0 11
	MAZ543_TEL 12 27
	MAZ543_Decoy 28 43
	M50_Tank 44 55
	M35_Truck 56 67
	UHaul_Truck 68 70
	Tree_Canopy 71 88

by converting the wavenumber to wavelength. Since the step size between the wavenumbers of the data is approximately 3.85 cm^{-1}, the spacing of actual data points in wavelength is about 80 nm at 14.2 μm and 3 nm at 3.0μm. Since the program finds the nearest actual data point when searching by wavelength, the difference between the nominal wavelength and that for which the data actually exists will be at most plus or minus half these values at the two extremes of the spectrum. This effect is seen in the labeling of the axes of the scatterplots for the trees in Figure 3. The nominal wavelengths which were entered to produce the plots were 3, 4, and 5 microns in the MWIR and 11, 12, and 13 microns in the LWIR. The closest wavelengths to each of these for which data was actually present in the collection are those used in the axis labels.

The decision to examine the data on the scale of wavelength rather than wavenumber was made for several reasons. First, the critical parameters, ρ and R, appeared to vary on the scale of wavelength rather than wavenumber. The change in the relationship between target and background was negligible when incrementing through the largest wavenumbers (the MWIR) but easily discernable for the lowest wavenumbers (the LWIR). In addition, filtering of the spectrum has been traditionally discussed in terms of wavelength, leading to the consideration of multispectral issues in a similar terms [7]. These reasons, along with the reduction in data processing provided by binning at intervals of wavelength, led to this choice, although examining the multispectral issue on the wavenumber scale could very well have provided additional insight during the course of this work.

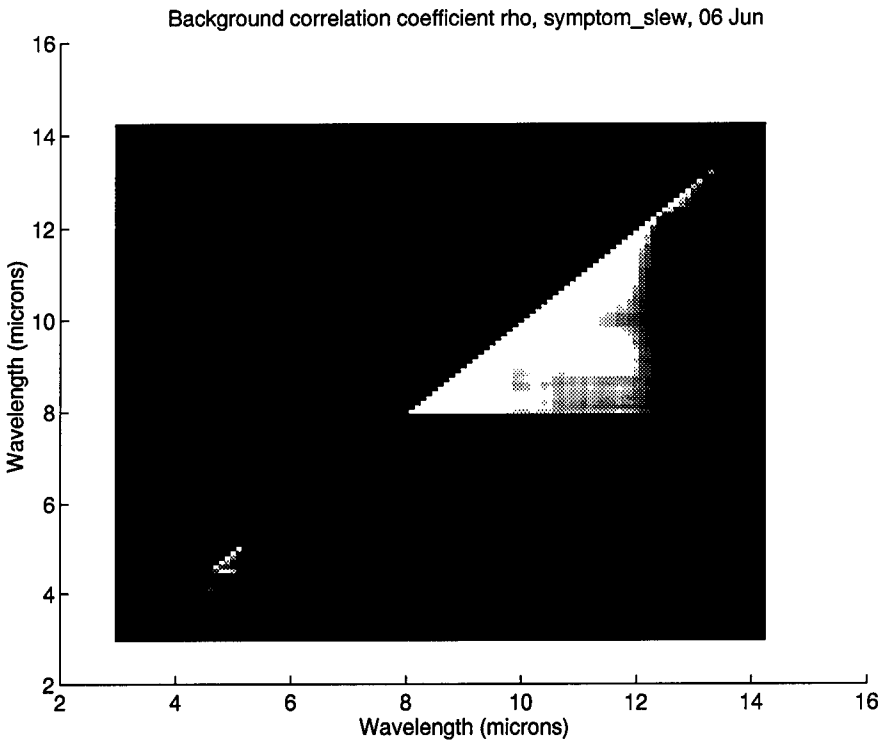

Figure 12. Wavelength map of the background ρ, 6-8 June 1994: *symptom_slew* Data Set

Figure 12 shows an intensity plot of the average background correlation for the tree canopy on June 6, 1994. Only the lower triangular half of the matrix of correlation values is shown, since the values are symmetric about a line at 45 degrees to either axis. The intensity scale for this figure is an inverse logarithmic function of the correlation value. The only wave bands which are distinguishable from the black background are those with ρ values of 0.97 or greater. The brightest regions in Figure 12 correspond to bandpairs exhibiting spectral correlations of 0.99 and higher. A very large fraction of the total wavelength pairs exhibited these high average correlations during 6–8 June.

The average color coefficient R across the dual-spectrum wavelength space for the M752 lance missile launcher and trees on 6 June is shown in Figure 13. The intensity for

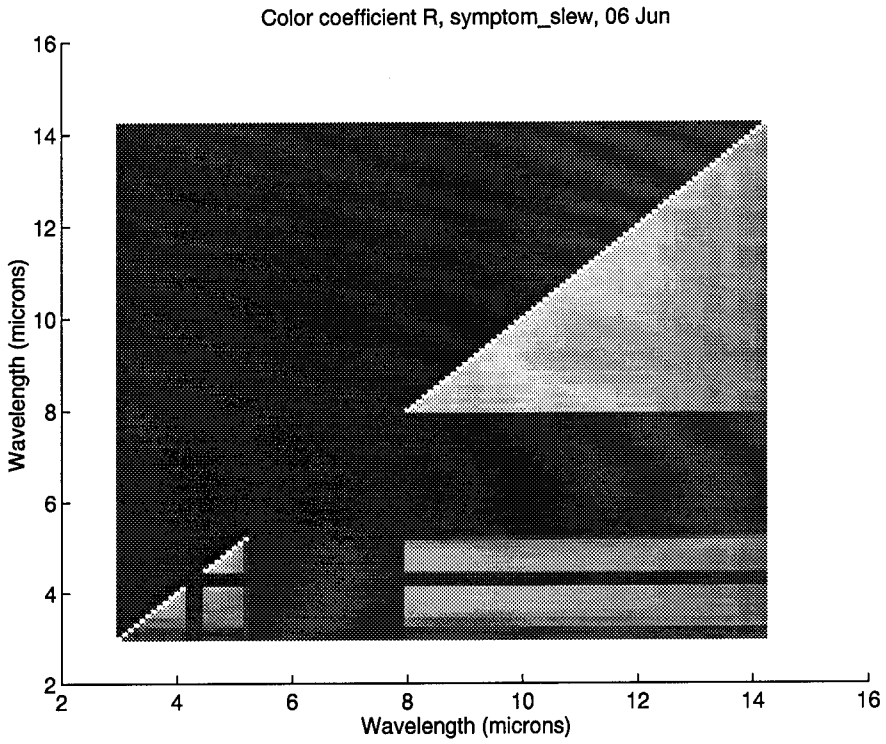

Figure 13. Wavelength map of the Color Ratio R, 6-8 June 1994: Lance Missile Launcher and trees, *symptom_slew* Data Set

the upper half of the dual-wavelength space indicates an R value of zero. The dark regions which cut through the middle of the spectrum are spectral wavelengths which are not passed by the atmosphere, and which are therefore not processed. The narrow band from 4.2 to 4.4 microns corresponds to a CO_2 molecular absorption line, while the larger region which has been removed from consideration is the range 6.0–7.9 microns, an absorption region due to water. These bands were also removed from consideration in the data depicted in Figure 12 as well, but their omission is less noticeable due to the dark surrounding regions in that figure. Note that for this target and background combination, there are no negative values of R.

4.1 The Statistics of the Symptom Slew collection

It is apparent from a comparison of Figures 12 and 13 that high correlations and high color (lower and negative R values) for this target and this background are somewhat mutually exclusive events. The following figure contains three scatterplots of all 3403 bandpairs considered in the MW, LW and MW/LW IR regions for the Lance and the trees. The figures of merit are again R and ρ averaged over the five collection times for each of the three days in June. These plots show how the target/background combination has a strong tendency

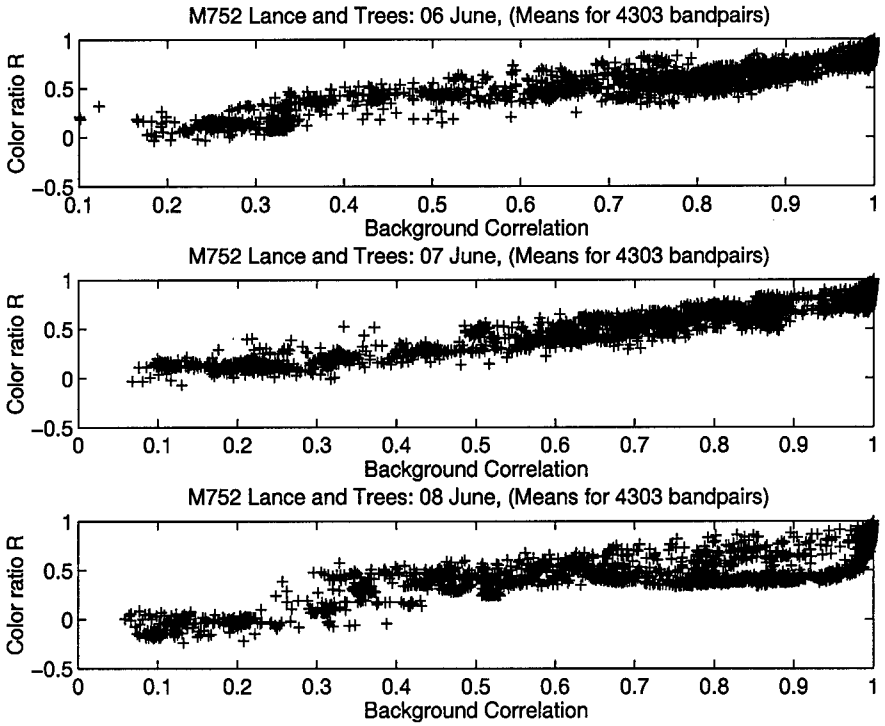

Figure 14. Relation between R and background ρ for 3403 bandpairs, 6-8 June 1994: *symptom_slew* Data Set

toward a loss of color with increasing background correlation between bands. Similar plots have been observed for all the other targets from 6–8 June with respect to the same tree

background. In general, the loss of color with increasing background correlation is evident in nearly all data of the *symptom_slew* collection.

Most IR detectors in use today in the region of 3–14 microns perform well only in either the long- or mid-wave IR. Therefore, it is natural to examine the properties of MW/MW LW/LW and MW/LW bandpairs separately, since a single detector in an operational sensor design may only cover a portion of the thermal infrared spectrum. The high background correlations which are deemed necessary for reliable target detection performance might be found for pairs in any, all, or none of the MW, LW and MW/LW regions. To characterize the background correlation levels of each region, the number of bandpairs for which $\rho \geq 0.99$ were counted for each time of day in the experiments of Table 2. These numbers were then divided by the total number of pairs from each region, 190 MW pairs, 1,953 LW pairs, and 1260 MW/LW pairs. These percentages are listed in Table 4.

4.2 Selection by SCR v. Selection by Score

Besides providing information on some of the important parameters involved with multispectral detection, the *symptom_slew* experiments were used to evaluate the performance of the *score* of Equation 24 in choosing bandpairs which consistently displayed high SCRs. The expression for the SCR of the perfectly matched spectral filter was used as the metric to evaluate the performance of each of the 3403 band combinations in each of the regions of the sampled spectra, and the value of the ratio was converted to dB ($20log_{10}(SCR)$). This evaluation was performed for each of the twenty targets versus the tree background for the

Table 4. Percentage of Bandpairs in each IR region with Background Correlation $\rho \geq 0.99$

Experiment Name	MW	LW	MW/LW
d06nz1	14.21	24.63	0
d06nz2	16.32	24.58	0
d06nz3	25.26	52.28	0
d06nz4	32.63	67.43	0
d06nz5	36.84	69.18	0
d07nz1	13.68	29.03	0
d07nz2	20.00	37.48	0
d07nz3	17.37	30.31	0
d07nz4	22.63	48.64	0
d07nz5	27.37	61.29	0
d08nz1	14.21	35.07	0
d08nz2	14.74	19.41	0
d08nz3	26.32	51.51	0
d08nz4	27.37	83.56	18.33
d08nz5	25.26	54.74	0

five collection times during the respective days, producing 100 separate lists of the calculated signal-to-clutter ratios for the 4303 bandpairs. In general, the highest SCRs were produced by pairs exhibiting very high background correlations ($\rho \geq 0.99$) and moderate degrees of color (R> 0.5). Occasionally, very poorly correlated bands with very good color (R< 0) produced the highest SCRs, as did bands with moderate color (R slightly above 0) and lower correlations ($\rho \geq 0.9$).

The lists were subsequently reduced in size and ranked by the following three conditions: 1) Ranked lists were produced based upon the overall SCR performance (average) for each of the three days, 2) Only pairs with background correlations greater than 0.99 were considered, 3) Only pairs providing an average SCR of 18 dB or greater over each day were considered. The number of pairs which met all three criteria ranged from approximately 300 to 700, depending on the target and time of day. These pairs were ranked first by calculating the mean SCR value during the day, then by the score of Equation 24. The lower bound T_b was chosen to be 18 dB because, assuming that Gaussian statistics describe the distributions, SCRs of 18 dB and above are generally expected to provide reliable target detection performance [7, 13, 18]. The differences between the rankings produced by the two methods were significant. The two methods typically exhibited only 70% commonality for a given number of the top ranked pairs, and the exact ordering of these was usually different.

The most straightforward and meaningful way to evaluate the two selection methods is to examine the SCRs for the different times of day which produced the rankings. The twenty ranked lists were based upon the five detection times for each of the three days.

Figures 15–20 on the following pages show how the pairs selected by *score* compare to those selected by average SCR for the top 10 pairs and top 50 pairs from each. Figures 15 and 16 concern the average SCRs present in the top 10 and 50 pairs, respectively, for all 100 detection scenarios (20 target/background matchups $\times$ the 5 times of day). In the upper half of each figure, the signal-to-clutter ratios which were placed in each final list are plotted versus the mean SCR between the two lists. As mentioned, the dual-band SCR is used here to provide some measure of the probable detection performance which might be expected for a given target and background. The range of values in which the highest SCRs fall for any detection opportunity thus gives an indication of the ease with which a sensor might detect the target. The mean SCR for the two methods plotted in the top graph of each figure is therefore plotted along the horzontal axes of both graphs as an indicator of the target detectibility for each of the 100 detection opportunities.

The lower portions of the figures are plots of the difference between the mean of the SCRs for the pairs which survived the two ordering processses. The value plotted for the average-SCR method is subtracted from that for the scoring method. Positive values in the lower plots correspond, therefore, to instances when the scoring method produced a 'better' list, as evaluated by the average of the SCRs, as well as the minimum and maximum SCR values, present in each list. The first two figures show that when the data reflects more difficult target detection circumstances, the scoring method tends to produce rank-ordered lists of bandpairs which, on average, have higher SCRs. Figures 17–20 show a similar trend

with regard to the best and worst SCRs evident in the lists. Again, using the scoring method is shown to be advantageous when the data reflect more difficult detection conditions.

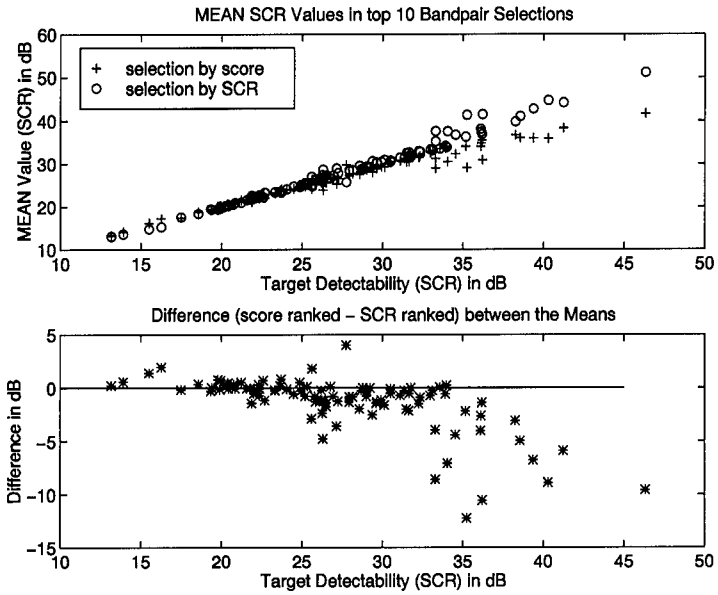

Figure 15. Comparison of Mean SCR values for top 10 bandpairs as rated by score and SCR: 100 detection opportunities from 6-8 June 1994: *symptom_slew* Data Set

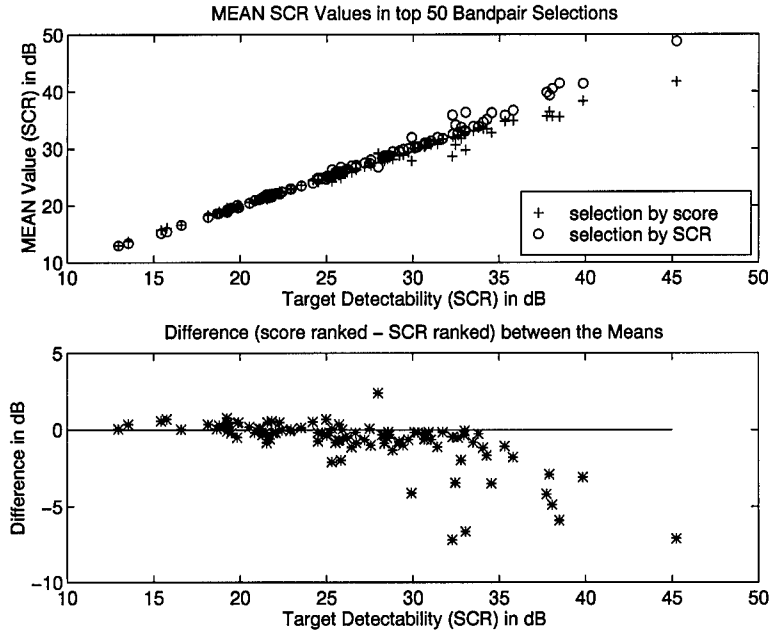

Figure 16. Comparison of Mean SCR values for top 50 bandpairs as rated by score and SCR: 100 detection opportunities from 6-8 June 1994: *symptom_slew* Data Set

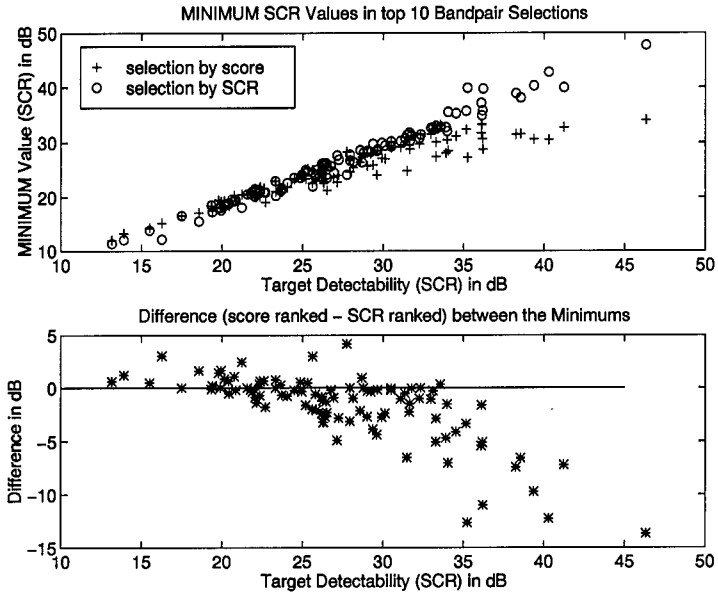

Figure 17. Comparison of Minimum SCR values for top 10 bandpairs as rated by score and SCR: 100 detection opportunities from 6-8 June 1994: *symptom_slew* Data Set

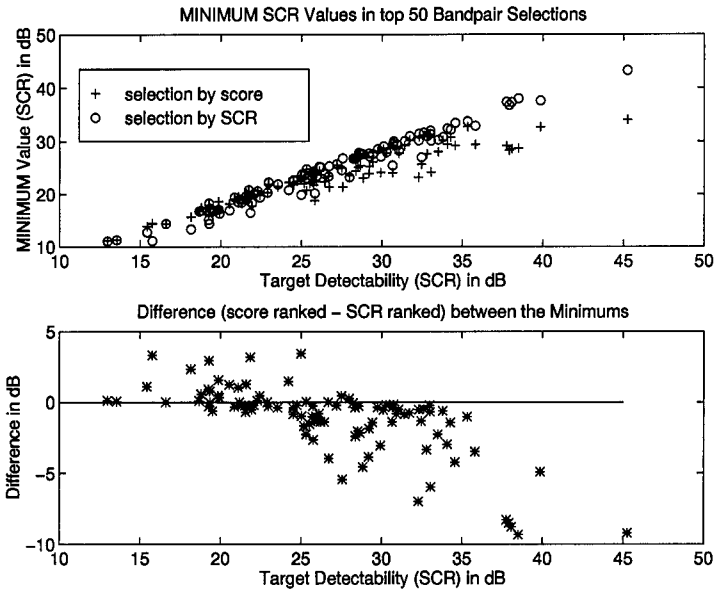

Figure 18. Comparison of Minimum SCR values for top 50 bandpairs as rated by score and SCR: 100 detection opportunities from 6-8 June 1994: *symptom_slew* Data Set

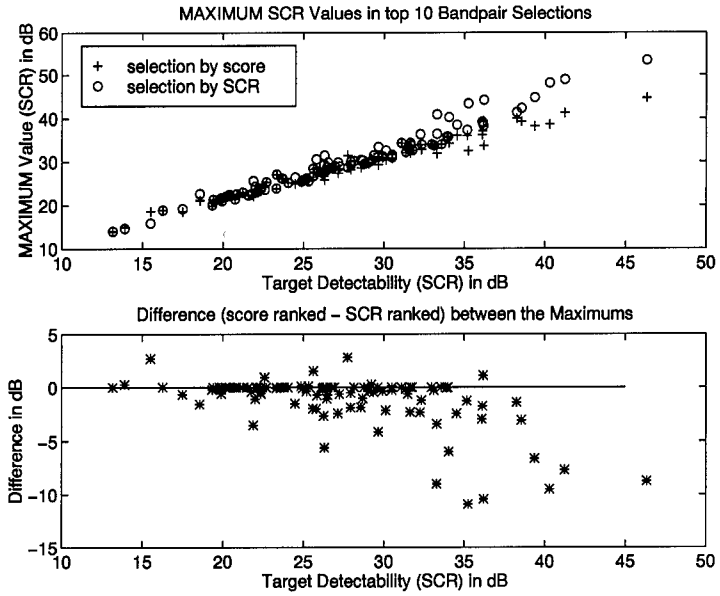

Figure 19. Comparison of Maximum SCR values for top 10 bandpairs as rated by score and SCR: 100 detection opportunities from 6-8 June 1994: *symptom_slew* Data Set

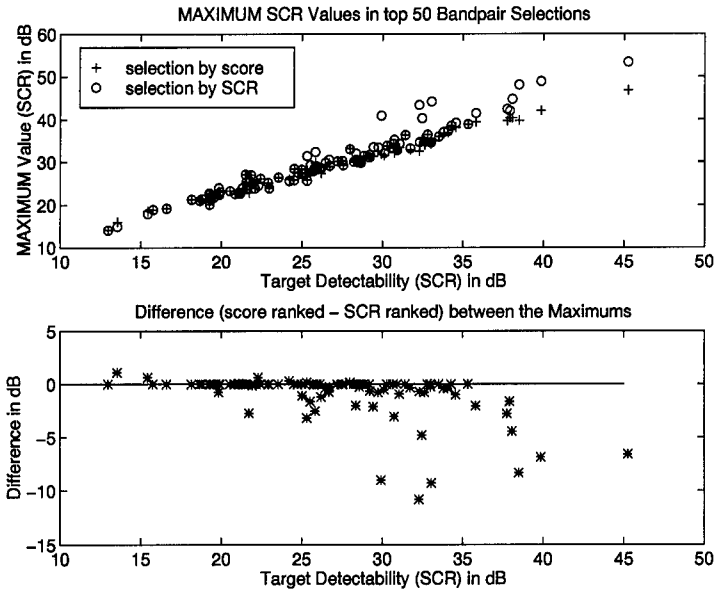

Figure 20. Comparison of Maximum SCR values for top 50 bandpairs as rated by score and SCR: 100 detection opportunities from 6-8 June 1994: *symptom_slew* Data Set

Another process used to evaluate the selection capabilities of the two methods involved detecting the target pixels at the wavelengths specified by the two different rankings. The lists produced by both methods were compared band-for-band through the top ten and thirty selections by re-accessing the spectral data for the two pairs and attempting detection of the target pixels using the minimum clutter (MC) processor. The detection method was simplified by dropping ρ from the second element of the weight vector used by the MC processing (Equation 15), since all correlations were greater than 0.99. The performance of each pair was evaluated based upon the number of target pixels which were successfully detected, as well as the incorrect target classifications (false alarms) made under H_1 and H_0 hypotheses. Detection was attempted for each target pixel individually (againt all background pixels) so that the presence of a proportionately large number of target pixels would not adversely affect estimates of the background clutter standard deviations. This is reasonable because the number of target pixels in the pre-processed image frames of interest will almost always be much less than the number of background pixels. A detection threshold was set at 1.75 times the standard deviation of the residual vector under H_1 for the comparison. This value was chosen when noting, after trial and error, that use of this value allowed pixels of both types to be mis-classified during the detection process. This allowed a comparison of the two methods based upon numbers of correctly identified target pixels as well as the number of tree pixels which were incorrectly classified as targets.

The scores and mean SCRs for each of the three days were used to select final pairs for the six target types. The final bandpair list for each target which guided the detection

process was a composite list that was compiled using the bandpair rankings from all days. Although data for the MAZ543 TEL exists for 7 June, this data was left out of consideration when making the final lists and detecting the MAZ543 because the engine of the vehicle was running during the collection on this day, whereas this target was cold on both 6 and 8 June [7].

The composite bandpair lists were used to detect the target pixels in each of the experiments involving the six target/background scenarios. Detection was performed using both the SCR and *score* composite lists for the top ten and thirty bandpairs. This amounts to (80 experiment times during the 3 days) $*$(2 ranking methods) $*$ [(10 pairs) + (30 pairs)] = 6,400 cases of target detection. The method of the list which came out on top in this evaluation are given in Tables 5 and 6. The SCR method is shown to perform better overall. This is the expected result, given the trends observed in the previous section. Since the lists of scored bandpairs exhibit a lower average SCR as the detectability of the targets increases, the predominance of such very good detection opportunities in the 100 cases which were examined gives rise to the results of Tables 5 and 6.

Table 5. Method Performance: Comparison of top TEN bandpairs

Experiment Name	M752 Lance	MAZ543 TEL	MAZ543 Decoy	M50 Tank	M35 Truck	U-Haul
d06nz1	SCR	score	SCR	tie	SCR	-
d06nz2	SCR	score	score	SCR	SCR	-
d06nz3	score	score	SCR	tie	tie	-
d06nz4	tie	SCR	SCR	tie	SCR	-
d06nz5	SCR	tie	SCR	tie	SCR	-
d07nz1	SCR	-	SCR	score	SCR	score
d07nz2	SCR	-	SCR	tie	SCR	tie
d07nz3	SCR	-	score	tie	tie	tie
d07nz4	tie	-	SCR	SCR	tie	score
d07nz5	tie	-	SCR	tie	tie	tie
d08nz1	score	SCR	SCR	tie	SCR	score
d08nz2	score	SCR	SCR	tie	SCR	score
d08nz3	tie	score	SCR	tie	tie	score
d08nz4	tie	SCR	SCR	tie	SCR	tie
d08nz5	SCR	score	SCR	SCR	tie	tie
Overall Result	SCR	score	SCR	SCR	SCR	score

Table 6. Method Performance: Comparison of top THIRTY bandpairs

Experiment Name	M752 Lance	MAZ543 TEL	MAZ543 Decoy	M50 Tank	M35 Truck	U-Haul
d06nz1	SCR	score	SCR	SCR	tie	-
d06nz2	SCR	score	tie	SCR	SCR	-
d06nz3	tie	score	SCR	score	score	-
d06nz4	tie	SCR	SCR	SCR	SCR	-
d06nz5	SCR	SCR	SCR	SCR	SCR	-
d07nz1	tie	-	SCR	score	tie	score
d07nz2	tie	-	SCR	score	SCR	tie
d07nz3	SCR	-	score	SCR	tie	SCR
d07nz4	score	-	SCR	tie	score	score
d07nz5	tie	-	SCR	SCR	tie	score
d08nz1	score	SCR	SCR	tie	SCR	SCR
d08nz2	score	score	SCR	SCR	score	score
d08nz3	score	tie	SCR	SCR	tie	score
d08nz4	score	SCR	SCR	tie	SCR	tie
d08nz5	tie	SCR	SCR	tie	tie	SCR
Overall Result	score	SCR	SCR	SCR	SCR	score

V. *Conclusions and Recommendations*

The *symptom_slew* data show large regions of high correlation for band pairings in the thermal IR. This fact suggests that multispectral detectors will often encounter background correlations which provide for good detection performance. In every experiment the LWIR exhibited a higher degree of correlation than the MWIR, while the MW/LW rarely exhibited sufficiently high ρ. The LWIR may therefore be a better region than the MWIR for providing reliable and accurate multispectral detection if $\rho \geq 0.99$ is a necessary condition.

The plots of Figure 14 show the disappointing loss of target/background color with increasing correlation, supporting similar observations which have been made after an examination of earlier JMSP data collections. The best SCRs typically are produced by highly correlated wavelength pairs, but this is not uniformly the case. The choice in this work of establishing the threshold for consideration of a bandpair at 0.99 for the background correlation often eliminated numerous MWIR pairs which had slightly lower ρ values but sufficient color (low R) to provide the highest SCRs. The highest number of MWIR pairs on any candidate list (of several hundred total pairs meeting the criteria $\rho \geq 0.99$ and SCR$\geq$ 18 dB) was twelve, and only occasionally were MWIR pairs included in the top 10, 30, or 50 bandpairs in the final ranked lists. The fact that many MWIR pairs with high SCRs were eliminated by this consideration of ρ suggests that the preference for the very highest correlations may be unjustified given the current assumption, made by proponents of the RX detection algorithm, that the covariance matrices of the background clutter distibutions may be accurately

estimated from actual sensor data in real-time with Equation 23. The dual-band SCR may alone be good enough for evaluating combinations of spectral bands. At the least, this work suggests that it may be necessary to re-examine the reasons for the bias toward extremly high correlations, which has sometimes been evidenced in previous research ([13] and [14]). Selecting bandpairs based upon a ranking accomplished with the score of Equation 24 shows an advantage when the data reflects difficult detection by exhibiting lower signal-to-clutter ratios. When the SCRs are higher, the disadvantage of the score-selected bandpairs should not be of great concern due to the still-excellent detection potential implied by the high SCRs. The score developed in this work could prove useful in evaluating the current and future multispectral data collections by directing the selection of spectral bandpairs which provide more consistent detection when the detection problem is more difficult. The use of the score is therefore recommended based upon the evidence developed during this work and presented in this thesis.

Appendix A. Listings of Experiments for the JMSP Multispectral Data Collections

wsmr experiments

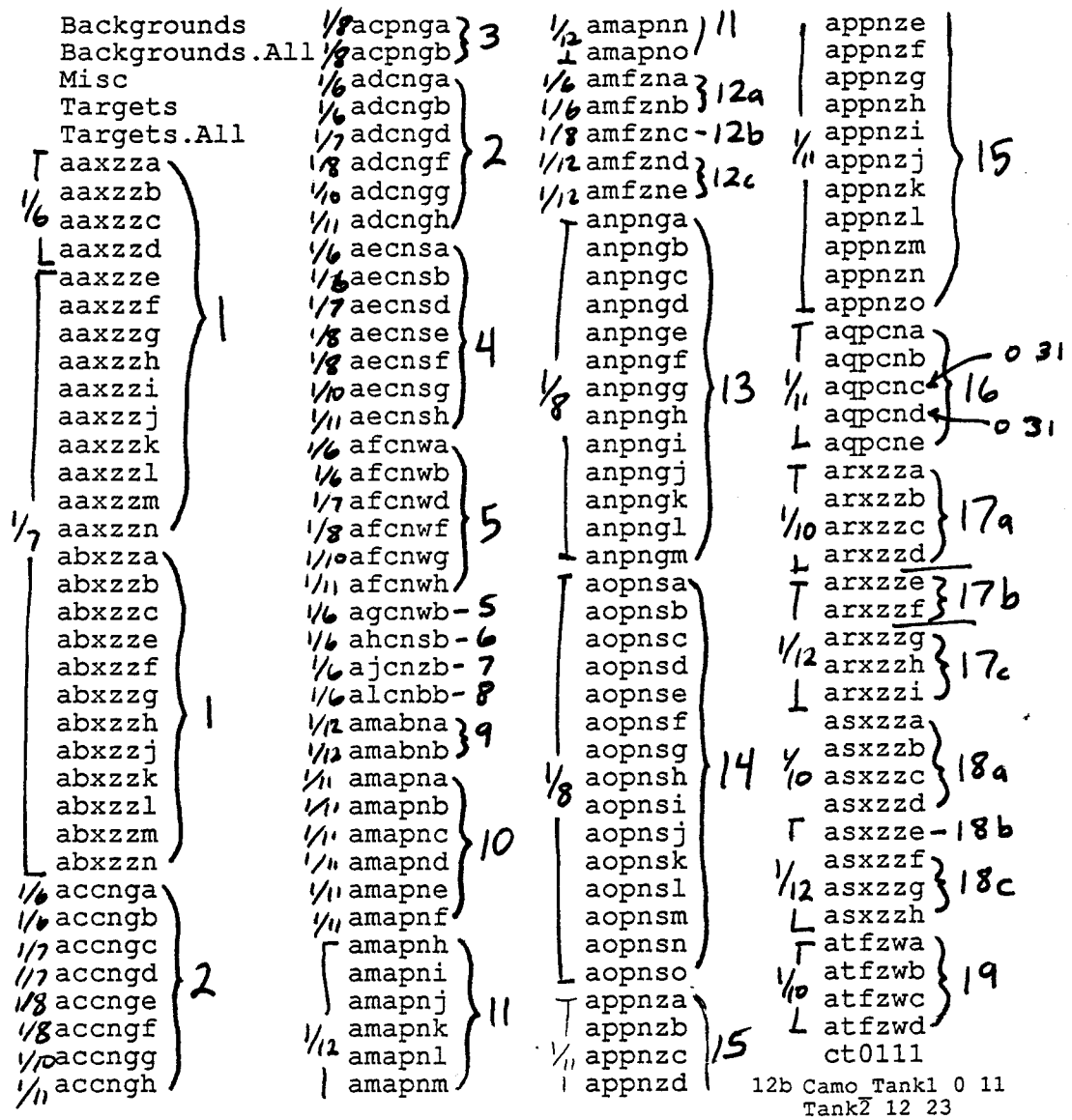

1 Tank1 0 11
Truck 12 23
CARC_Tan 24 25
Low_E_Tan 26 27
Diffuse 28 29
Specular 30 31
CARC_Green 32 33
Sky 34 38
Blackbody 39 41
Scrub 42 71

2 Grassy_Area 0 29

3 Grassy_Area 0 63

4 Bare_Soil 0 29

5 Mesquite_Bushes 0 29

6 Turned_Soil 0 29

7 Mixed_Backgrounds 0 29

8 Bushes 0 29

9 Sky 0 4
Blackbodies 5 7

10 CARC_Tan 0 1
Low_E_Tan 2 3
Diffuse 4 5
Specular 6 7
CARC_Green 8 9
Sky 10 14
Blackbodies 15 17

11 CARC_Tan 0 1
Low_E_Tan 2 3
Diffuse 4 5
Specular 6 7
CARC_Green 8 9

12a Tank1 0 11
Tank2 12 23
Truck 24 35
Hertz_Truck 36 47
BB_Trailer 48 59
CARC_Tan 60 61
Low_E_Tan 62 63
Diffuse 64 65
Specular 66 67
CARC_Green 68 69
Sky 70 74
Blackbody 75 77

12b Camo_Tank1 0 11
Tank2 12 23
Camo_Truck 24 35
Hertz_Truck_Cab 36 38
Hertz_Truck_Back 39 50
BB_Trailer 51 62
White_Truck 63 74
Camo_CARC_Tan 75 76
Camo_Low_E_Tan 77 78
Diffuse 79 80
Specular 81 82
CARC_Green 83 84
Camo_Cylinder 85 86
Sky 87 91
Blackbody_OFF 92 94

12c Camo_Tank1 0 11
Tank2 12 23
Truck_Canvas 24 27
Truck_Cab 28 32
Truck_Side 33 35
Hertz_Truck_Cab 36 38
Hertz_Truck_Back 39 50
BB_Trailer 51 62
White_Truck 63 74
CARC_Tan 75 76
Low_E_Tan 77 78
Diffuse 79 80
Specular 81 82
CARC_Green 83 84
Cylinder 85 86
Sky 87 91
Blackbody 92 94

13 Grassy_Area 0 63

14 Soil 0 63

15 Scrub 0 63

16 Camo_Tank1 0 15

17a Camo_Tank1 0 11
Camo_Truck 12 23
Camo_CARC_Tan 24 25
Camo_Low_E_Tan 26 27
Diffuse 28 29
Specular 30 31
CARC_Green 32 33
Camo_Cylinder 34 35
Sky 36 40
Blackbody 41 43
Soil 44 73

17b Tank2 0 11
Truck_Canvas 12 15
Truck_Cab 16 20
Truck_Side 21 23
CARC_Tan 24 25
Low_E_Tan 26 27
Diffuse 28 29
Specular 30 31
CARC_Green 32 33
Cylinder 34 35
Sky 36 40
Blackbody 41 43
Soil 44 73

17c Targets of 17b plus
T72_Tank 0 11

18a Camo_Tank1 0 11
Camo_Truck 12 23
Camo_CARC_Tan 24 25
Camo_Low_E_Tan 26 27
Diffuse 28 29
Specular 30 31
CARC_Green 32 33
Camo_Cylinder 34 35
Sky 36 40
Blackbody 41 43
Scrub 44 73

18b Tank2 0 11
Truck_Canvas 12 15
Truck_Cab 16 20
Truck_Side 21 23
CARC_Tan 24 25
Low_E_Tan 26 27
Diffuse 28 29
Specular 30 31
CARC_Green 32 33
Cylinder 34 35
Sky 36 40
Blackbody 41 43
Scrub 44 73

18c Targets of 18b plus
T72_Tank 0 11

19 Camo_Tank1 0 11
Tank2 12 23
Camo_Truck 24 35
Hertz_Truck_Cab 36 38
Hertz_Truck_Back 39 50
BB_Trailer 51 62
White_Truck 63 74
Rental_Car 75 82
CARC_Tan 83 84
Low_E_Tan 85 86
Diffuse 87 88
Specular 89 90
CARC_Green 91 92
Cylinder 93 94
Sky 95 99
Blackbody 100 102
Scrub 103 132

micom experiments

Backgrounds
Backgrounds.All
Misc
Targets
Targets.All

9/10 ct0716
8/9 ct0717
7/19 ct0719
7/20 ct0720
7/21 ct0721
7/22 ct0722
} 1

10/6 m1c0c0 - 2
7/16 m1ckt0 - 3
m1mkta - 4
7/14 m1mlta
m1mltb
m1mltc
} 5

7/17 m1mltf
7/17 m1mltg
} 6

7/14 m1mpta
7/14 m1mptb
7/14 m1mptc
} 7

7/16 m1mptd - 8
8/13 m1mpte
8/13 m1mptf
7/17 m1mptg
7/17 m1mpth
} 9

7/12 m1mtt0 - 10
7/14 m1mzta - 11
8/26 m2mpt0 - 12
7/19 m2mpt1 } 12

7/17 m3c0t0 - 13
7/17 m3mvt0 - 14
8/26 m3mz00 - 15
7/19 m4cj00 - 16
7/17 m5mtc0 - 17
7/19 m5mtca - 18

m6mpta
m6mptb
7/19 m6mptc
m6mptd
m6mpte
} 19

m7mtta
m7mttb
m7mttc
7/19 m7mttd
m7mtte
m7mttf
} 20

m7mzt0
m7mzta
m7mztb
m7mztc
7/20 m7mztd
m7mzte
m7mztf
m7mztg
} 21

7/19 m8mz00 - 22
7/16 mac0d0
7/17 mac0d1
7/16 mac0da
} 23

7/20 map0d0 - 24
7/19 mbc0t0
7/19 mbc0t1
} 25
7/16 mbc0ta

7/17 mcc0c0
7/17 mcc0ca
} 26
7/16 mcc0cb

7/16 mcp0ca
7/17 mdc0c0
} 27
7/16 mdc0ca

mec0g0
7/19 mec0ga
} 28
7/19 memzz0 - 29
7/17 mfcjg0 - 30

7/21 mfmpt0
7/22 mfmpt2
} 31
7/22 mfmpt3

7/22 mfmpt4
7/22 mfmpt5
} 32
7/21 mfmpta - 33
7/21 mfmptb - 33 + Cylinder 6 7
7/22 mfmptc
7/22 mfmptd } 33 + cyl 6 9

7/21 mfte00
7/22 mfte01
7/22 mfte02
} 34

7/21 mgc0d0 - 35
7/21 mgc0r0
7/22 mgc0ra
} 36
7/21 mgc0s0 } 37

7/21 mgc0sa - 37
7/21 mgc0z0 - 38
mhmtca - 39a
mhmtcb
mhmtcc
7/21 mhmtcd
mhmtce
mhmtcf
mhmtcg
mhmtch
mhmtcj
mhmtck
mhmtcl
mhmtcm
7/22 mhmtcn
mhmtco
mhmtcp
mhmtcq
mhmtcr
} 39b

7/21 mic0z0 - 40
mjc0z0 - 41
mkmzz0 - 42

mzp0z0
mzp0z1
7/20 mzp0z2
mzp0z3
mzp0z4
} 43

1 Blackbodies 0 29

2 Tree_Canopy 0 31

3 Camo_Truck 0 17
Transition 18 33

4 Tree_Canopy 0 8
Camo_Truck 9 18
Gravel_Road 19 22
Transition 23 31

5 Tree_Canopy 0 8
Diffuse_Panel 9 10
Low_E_Panel 11 12
Specular_Panel 13 14
Gravel_Road 15 18
Transition 19 27

6 Diffuse_Panel 0 0
Low_E_Panel 1 1
Specular_Panel 2 2
Transition 3 38

7 Tree_Canopy 0 8
Diffuse_Panel 9 10
Painted_Panel 11 12
Specular_Panel 13 14
Gravel_Road 15 18
Transition 19 27

8 Tree_Canopy 0 15
Diffuse_Panel 16 17
Painted_Panel 18 19
Specular_Panel 20 21
Transition 22 37

9 Diffuse_Panel 0 0
Painted_Panel 1 1
Specular_Panel 2 2
Transition 3 38

10 Trees 0 8
Truck 9 18
Road 19 22
Transition 23 31

11 Tree_Canopy 0 8
Hydice_L 9 10
Hydice_U 11 12
Cylinder 13 14
Box 15 16
Gravel_Road 17 20
Transition 21 29

12 Painted_Panel 0 1
Environment 2 9

13 Road 0 15
Grass 16 31
Trees 32 47

14 Van 0 7
Underbrush 8 23
Grass 24 31
Gravel_Road 32 39

15 Hydice_L 0 1
Hydice_U 2 3

16 Junk 0 25

17 Truck 0 5
Trees 6 21

18 Truck 0 5
Trees 6 20

19 Painted_Panel 0 1
Tree_Canopy 2 17

20 Truck_Cab 0 3
Truck_Canvas 4 10
Transition 11 46

21 Low_E_Panel 0 1
Mat_Camo 2 3
Painted_Panel 4 5
Exp_Net 6 41
Transition 42 77

22 Barrels 0 2
Camo_Boxes 3 6
Building_1 7 11
Building_2 12 20
Eqpt_Racks 21 25

23 Tree_Canopy 0 35
24 Tree_Canopy 0 69
25 Transition 0 31
26 Tree_Canopy 0 35
27 Tree_Canopy 0 31
28 Soil/Grass 0 35

29 Truck_1 0 2
Truck_2 3 5
Tank_1 6 10
Trailer 11 14
APC 15 17
Tank_2 18 21
Grass\Soil 22 37
Tree_Canopy 38 53

30 Junkyard 0 31

31 Diffuse_Panel 0 1
Painted_Panel 2 3
Specular_Panel 4 5
Cylinder 6 7
Trees 8 16
Grass 17 25
Sky 26 30

32 Diffuse_Panel 0 1
Painted_Panel 2 3
Specular_Panel 4 5
Cylinder 6 11
Grass 12 20
Trees 21 29
Sky 30 34

33 Diffuse_Panel 0 1
Painted_Panel 2 3
Specular_Panel 4 5
Trees 6 14
Grass 15 23
Sky 24 28

34 Diffuse_Panel 0 1
Emissive_Panel 2 5
Specular_Panel 6 7
Sky 8 12

35 Tree_Canopy 0 35
36 Gravel_Road 0 29
37 Soil 0 29
38 Mixed_Background 0 3

39a Truck 0 9
Trees 10 45
39b Painted_Panel 0 1
Truck 2 11
Trees 12 47

40 Mixed_Forest 0 35
41 Mixed_Background 0 3

42 Bridge 0 4
River 5 9
Trees 10 14

43 Mixed_Background 0 6

wright_lab experiments

Backgrounds
Backgrounds.All
Targets
Targets.All
a09241-1
a09301
a09302
a09303
a09304
a09305
a09306
} 1
a10071
a10072
a10073
a10074
a10075
a10076
a10077
a10078
} 1
a10141
a10142
a10143
a10144
a10145
} 2
a10221
a10223
a10225
a10227
a10229
a1022b
} 2
a10281
a10283
a10285
} 2
a11091
a11093
a11095
} 2
a11291
a11293
a11295
} 2
b09241
b09301
b09302
b09303
b09304
b09305
} 1
b10071
b10072
b10073
b10074
b10075
b10076
b10077
b10078
} 1
b10141
b10142
b10143
b10144
b10145
} 2
b10222
b10224
b10226
} 2

b10228
b1022a
b1022c
} 2
b10282
b10284
b10286
} 2
b11092
b11094
} 2
b11222
b11224
b11226
} 2
b11292
b11294
} 2
c09305-3
c10075
c10077
} 3
c10145-3
c10221
c10223
c10225
c10227
c1022a
} 3
c10281
c10283
c10285
} 3
c11091
c11093
c11095
} 3
c11222
c11224
c11226
} 3
c11291
c11293
} 3
d09301
d09303
d09305
} 4
d10071
d10073
d10075
d10077
d10078
} 4
d10143
d10145
} 4
d11221
d11223
d11225
} 4
d11294-4
e09241-5
e09301
e09302
e09303
e09304
e09305
} 5
e10071
e10072
e10073
e10074
e10075
e10076
e10077
e10078
} 6

e10141
e10142
e10143
e10144
e10145
} 6
e10222
e10224
e10226
e10228
e10229
e1022c
} 6
e10282
e10284
e10286
} 6
e11092
e11094
} 6
e11221
e11222
e11223
e11224
e11225
e11226
} 6
e11292
e11294
} 6
f10075-7
g10221
g10222
g10223
g10224
g10225
g10226
g10227
g10228
g10229
g1022a
g1022b
g1022c
} 4
g10281
g10282
g10283
g10284
g10285
} 4
g11092
g11093
g11094
g11095
} 4
g11221
g11223
g11225
} 4
g11291
g11292
g11293
g11294
} 4
h10221
h10222
h10223
h10224
h10225
h10226
h10227
h10228
} 8

h10229
h1022a
h1022b
h1022c
} 8
h10281
h10282
h10283
h10284
h10285
} 8
h11091
h11092
h11093
h11094
h11095
h11096
h11097
} 8
h11221
h11222
h11223
h11224
h11225
h11226
h11227
} 8
h11291
h11292
h11293
h11294
} 8
i10221
i10222
i10223
i10224
i10225
i10226
i10227
i10228
i10229
i1022a
i1022b
i1022c
} 4
i10281
i10282
i10283
i10284
i10285
} 4
i11091
i11092
i11093
i11094
i11095
} 4
i11291
i11292
i11293
i11294
} 4
j11097-9
k11097-10
l11097
l11098
} 11
l11227-12
m11098-13
m11099-14

1 Mixed_Trees 0 35

2 Mixed_Trees 0 35
Diffuse_Panel 36 37
CARC_Panel 38 39
Specular_Panel 40 41

3 Grass 0 29

4 Mixed_Trees 0 71

5 Mixed_Trees 0 8
Diffuse_Panel 9 10
Black_Panel 11 12
CARC_Panel 13 14
Specular_Panel 15 16
Grass 17 25

6 Mixed_Trees 0 8
Diffuse_Panel 9 10
Emissive_Panel 11 12
CARC_Panel 13 14
Camo_Net 15 16
Specular_Panel 17 18
Grass 19 27
Obscured_Truck 28 31
Open_Truck 32 36

7 Flight_Line 0 1
AF_Museum 2 3
Concrete 4 5
Hangar_4B 6 7
Reactor 8 9
Gravel_Path 10 11

8 Diffuse_Panel 0 1
Emissive_Panel 2 3
CARC_Panel 4 5
Specular_Panel 6 7

9 Asphalt_Road 0 0

10 Brown_Grass 0 0
Dead_Leaves 1 1
Green_Grass 2 2
Green_Leaves 3 3

11 Sky 0 3

12 Sky 0 2

13 Soil_Car 0 1

14 Soil_Car_Exhaust 0 1

symptom_slew experiments

Backgrounds
Backgrounds.All
Targets
Targets.All
a06np1
a06np2
a06np3
a06np4
a06np5
a07np1
a07np2
a07np3
a07np4
a07np5
a08np1
a08np2
a08np3
a08np4
a08np5
b06ns1
b06ns2
b06ns3
b06ns4
b06ns5
b07ns1
b07ns2
b07ns3
b07ns4
b07ns5
b08ns1
b08ns2
b08ns3
b08ns4
b08ns5
c06ns1
c06ns2
c06ns3
c06ns4
c06ns5
c07ns1
c07ns2
c07ns3
c07ns4
c07ns5
c08ns1
c08ns2
c08ns3
c08ns4
c08ns5
d06nz1
d06nz2
d06nz3
d06nz4
d06nz5
d07nz1
d07nz2
d07nz3
d07nz4
d07nz5
d08nz1
d08nz2
d08nz3
d08nz4
d08nz5
e06np1
e06np2
e06np3
e06np4
e06np5
e07np1
e07np2
e07np3
e07np4
e07np5
e08np1
e08np2
e08np3
e08np4
e08np5
f06mz1
f06mz2
f06mz3
f06mz4
f06mz5
f07mz1
f07mz2
f07mz3
f07mz4
f07mz5
f08mz1
f08mz2
f08mz3
f08mz4
f08mz5
g06np1
g06np2
g06np3
g06np4
h09nz1
h09nz2
h09nz3
h09nz4
h09nz5
h09nz6
h09nz7
h09nz8
h09nz9
h09nza
h09nzb
h09nzc
h09nzd
i09nz1
i09nz2
i09nz3
i09nz4
i09nz5
i09nz6
i09nz7
i09nz8
i09nz9
i09nza
i09nzb
i09nzc
i09nzd
j09ns1
j09ns2
j10ns1
k10nz1
k10nz2
k10nz3
k10nz4
k10nz5
k10nz6
k10nz7
k10nz8
k10nz9
k10nza
k10nzb
k10nzc
k10nzd
k10nze

1 Specular_Panel 0 0
Diffuse_Panel 1 1
Black_Panel 2 2
CARC_Green_Panel 3 3
Blackbody 4 4
Sky 5 7

2 MAZ543_TEL 0 51

3 MAZ543_TEL 0 15
Tree_Canopy 16 51

4 M752_Launcher 0 11
MAZ543_TEL 12 27
MAZ543_Decoy 28 43
M50_Tank 44 55
M35_Truck 56 67
Tree_Canopy 68 85

5 M752_Launcher 0 11
Lance_Missile 12 14
MAZ543_TEL 15 30
Scud_B_Missile 31 34
MAZ543_Decoy 35 50
Scud_B_Decoy 51 54
M50_Tank 55 66
M35_Truck 67 78
UHaul_Truck 79 81
Tree_Canopy 82 99

6 M752_Launcher 0 11
MAZ543_TEL 12 27
MAZ543_Decoy 28 43
M50_Tank 44 55
M35_Truck 56 67
UHaul_Truck 68 70
Tree_Canopy 71 88

7 M752_Launcher 0 0
MAZ543_TEL 1 2
MAZ543_Decoy 3 4
M50_Tank 5 5
M35_Tank 6 6
Tree_Canopy 7 24

8 Specular_Panel 0 1

9 Specular_Panel 0 0
M50_Tank 1 12
M35_Truck 13 24
UHaul_Truck 25 27
Sky 28 30

10 CARC_Green_Panel 0 0
M752_Launcher 1 2
MAZ543_TEL 3 6
MAZ543_Decoy 7 10
Tree_Canopy 11 46

11 Specular_Panel 0 0
MAZ543_TEL 1 11
Dirt_Pile 12 27
Grass 28 59

12 Flightline 0 89

Appendix B. Guide to MATLAB Code and the Multispectral Data Format

B.1 Organization of the JMSP Data

The multispectral data used in this thesis was modified to be read by SUN microsystems's SPARC workstations in early 1994. It was provided in the tape archive file *bomem_raw.tar* which, when 'un-tared', creates a directory called *bomem* containing the data from the first three collections, each in its own subdirectory. The *symptom_slew* collection is retrieved by un-taring the file *symptom_slew.tar*. This file places the data from the fourth collection into directory *symptom_slew*, which can be moved into the *bomem* directory to allow access to all four sets through the same path.

The data from each experiment is given a separate directory which corresponds to the six-letter experiment name. The filenames within these are designated by the experiment name followed by a three-letter extension. The most important files are described below with one experiment from the wsmr data set used as an example:

Path	Description
/bomem/wsmr	The wsmr collection directory
/bomem/wsmr/asxzza	Directory containing files for experiment asxzza
/bomem/wsmr/asxzza/asxzza.raw	Spectral data for experiment asxzza
/bomem/wsmr/asxzza/asxzza.grt	Ground truth file listing targets and their locations within the raw data
/bomem/wsmr/asxzza/asxzza.hdr	Experiment header giving date and time of the experiment

The output of the ground truth file asxzza.grt is given below:

Table 7. Targets listed in asxzza.grt

Camo_Tank1 0 11
Camo_Truck 12 23
Camo_CARC_Tan 24 25
Camo_Low_E_Tan 26 27
Diffuse 28 29
Specular 30 31
CARC_Green 32 33
Camo_Cylinder 34 35
Sky 36 40
Blackbody 41 43
Scrub 44 73

The numbers after each target description give the locations in the raw data where the spectra from the target may be found. For experiment asxzza, there are 74 separate samples of various targets and backgrounds. Each sample consists of a 728-point spectrum produced by the MB-100 FTS collection instrument. Because of the nature of the collection instrument, the spectrum sample points are spaced at intervals of constant energy from 698.10553 cm^{-1} to 3502.09839 cm^{-1}. The spacing is therefore linear in wavenumber, but non-uniformly spaced in wavelength due to the inverse relationship between the two units of measure. The spacing between sample points in wavelength is approximately 0.5 nm at 2.86 microns and 80 nm around 14.32 microns.

The data in asxzza.raw is a single vector of numbers in IEEE floating point format. New code was developed to read and manipulate the JMSP data on The Air Force Institute of Technology's Sun Microsystems SPARC workstations. The MATLAB code written during

this thesis manipulates the data after it is first read into a single vector, $\underline{a}$. The indices for the targets in experiment asxzza, which are listed above, describe the location of the data for each vehicle within vector $\underline{a}$, as shown in Figure 21. The data for the camouflaged truck begins with the first point in spectrum number 12 and ends with the 728th point in spectrum 23. The twelve 'looks' at the truck taken during experiment asxzza therefore consitute 8,736 of the 53,872 elements in the data vector $\underline{a}$.

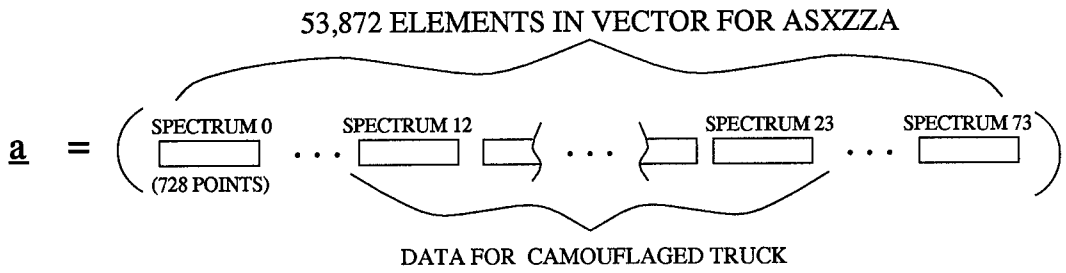

Figure 21. Location of Camo_Truck spectra in data vector $\underline{a}$

B.2 MATLAB File Descriptions and Outputs

The major and subsidiary MATLAB m-files used to manipulate the data are listed below with a brief description of each. More detailed descriptions of the individual files and sample outputs for most are given in the next section of this appendix.

Table 8. The Major MATLAB commands

Command	Use
main	select data set and a single experiment
new	select different experiment within chosen data set
grt	list the targets in an experiment
hdr	list the experiment collection date and time
target	define ranges in the data of all targets of interest (up to five)
sp	scatterplot of all targets at a single pair of wavelengths
d06nz_RUN1	multiple experiment target extraction guided by file 'testd06nz_M752'
multaccess	2D maps of SCR,R,G,and target and background correlation ρ
pairstats	Produces statistics for the bandpairs across the IR for a given experiment series with target and background
pairscores	Ranks top bandpairs by dual-band SCR and by score
finalpairs	Selects final lists of bandpairs based upon rankings for several data series by SCR and score. Then performs detection on original data as a comparison of the two bandpair lists

Table 9. Subsidiary MATLAB commands

Command	Use
access	Interface routine called by multaccess.m or used alone to interface with the figures produced by multaccess.m
rsp	Scatterplot routine called by access.m
suppress	Weighted band differencing routine called by access.m
bestbySCR_no_brho	Used by pairstats.m to rank bandpairs by dual-band SCR
bestpairs	Used by pairscores.m to rank bandpairs by dual-band SCR as well as score
finaldet	Used by finalpairs.m to perfom detection in the data for the bandpair selections as ranked in finalpairs.m

main

Typing this command from within the MATLAB program will produce either a graphical point-and-click menu or a text menu for use in selecting the data collection to be examined. When the data set is chosen, the file prompts for the experiment name and types the associated ground truth and header files (by running the m-files grt.m and hdr.m) after the data has been loaded, as shown by the following MATLAB screen output:

```
>> main

----- Choose desired data set: -----

      1) Micom
      2) WSMR
      3) Wright Labs
      4) Symptom_slew


Select a menu number: 4

Enter name of experiment ==> d06nz1

M752_Launcher 0 11
MAZ543_TEL 12 27
MAZ543_Decoy 28 43
M50_Tank 44 55
M35_Truck 56 67
Tree_Canopy 68 85


   698.10553  first wavenumber
  3502.09839  last wavenumber
   728.00000  number of points
```

```
     6  month
     6  day
     3  hour
    23  minute

>>
```

new

This command allows selection of a new experiment within the same data collection. MATLAB screen output looks like the following:

```
>> new

Enter name of experiment ==> a08np1

Specular_Panel 0 0
Diffuse_Panel 1 1
Black_Panel 2 2
CARC_Green_Panel 3 3
Blackbody 4 4
Sky 5 7


   698.10553  first wavenumber
  3502.09839  last wavenumber
   728.00000  number of points
           6  month
           8  day
           3  hour
          56  minute

>>
```

If the user invokes this command but reconsiders the decision to switch to another experiment, the operation can be canceled with an input of <Return>.

target

Use to select the indices to the targets and/or backgrounds of immediate interest. A maximum of five targets may be selected, and the command may be used to change these selections at any time without affecting the experiment data in memory. The example output reproduced below selects all radiometric measurements for three targets: the M752 Lance missile launcher, the M-50 tank, and the tree canopy background.

```
>> target

M752_Launcher 0 11
MAZ543_TEL 12 27
MAZ543_Decoy 28 43
M50_Tank 44 55
M35_Truck 56 67
Tree_Canopy 68 85


Enter ranges for all targets (e.g. for two targets: 0 9 24 47 ) ==> 0 11 44 55
68 85
>>
```

A single radiometric spectrum from each vehicle may be examined with respect to the trees as well. The following line selects the first spectrum in the data from each vehicle and all data for the trees:

```
Enter ranges for all targets (e.g. for two targets: 0 9 24 47 ) ==> 0 0 44 44
68 85
>>
```

sp

When the targets of interest have been selected from the experiment data, they may be repeatedly scatterplotted at any two wavelengths with the *sp* command. The three targets (2 vehicles, 1 background) chosen in the previous example are scatterplotted at 9 and 11 microns in the following example:

```
>> sp
1st wavelength? (between 2.86 and 14.25 microns) ==> 9
2nd wavelength? (in microns) ==> 11
blue_cross =
1st target

red_circle =
2nd target

magenta_star =
3rd target
>>
```

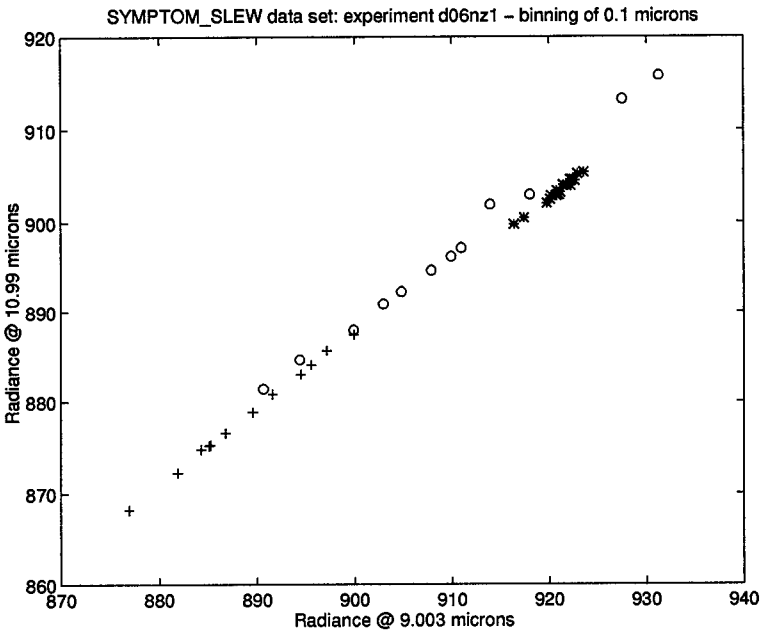

Figure 22. Scatterplot Produced by the Command *sp*

m-file **d06nz_RUN1.m** and text file **testd06nz_M752**

These two files together constitute the primary method for calculating the parameters important to multi-spectral detection for the JMSP data. After the text file is read by the m-file, the dual-band SCR, color ratio R, Multispectral gain G, and target and background correlations (ρ) are calculated for all pairings of wavelengths at 100 nm intervals from 3–14.2 microns and with 0.1 micron binning of the data. For convenience, the name of this m-file indicates that the code will calculate these parameters for the five experiments in series d06nz_ as directed by the text file testd06nz_M752. The contents of testd06nz_M752 are:

```
d06nz1 00 11 1
d06nz2 00 11 1
d06nz3 00 11 1
d06nz4 00 11 1
d06nz5 00 11 1

d06nz1 68 85 2
d06nz2 68 85 2
d06nz3 68 85 2
d06nz4 68 85 2
d06nz5 68 85 2
```

This text file guides the m-file in accessing the various experiments of the series and selecting the targets to be examined; in this case, the M752 Lance missile launch vehicle and tree background of the d06nz_ experiment series. The file must be created as shown in Figure B.3.

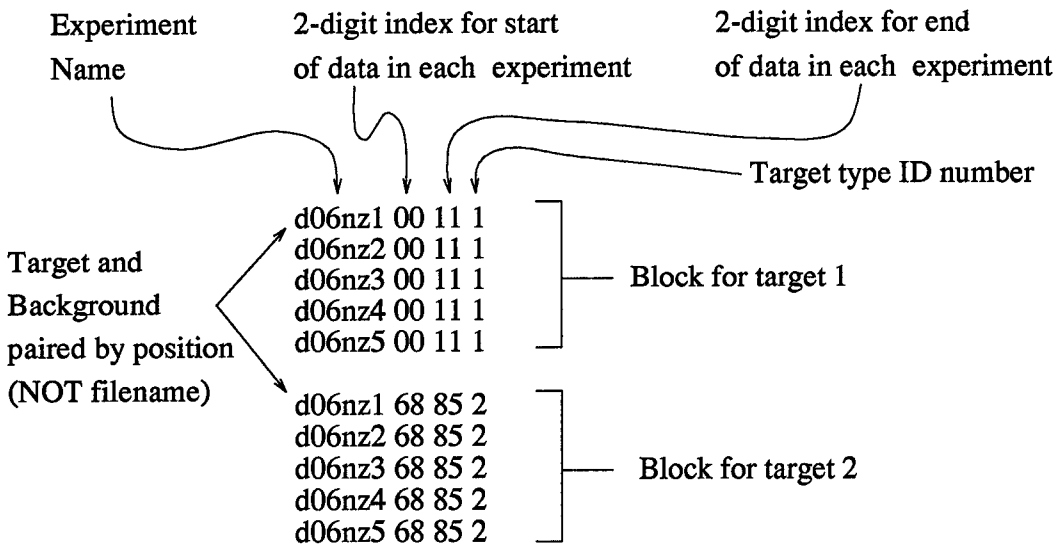

Figure 23. Format of text file testd06nz_M752 Which Directs m-file d06nz_RUN1.m

Given this format, a text file directing the examinination of the M50 tank data in experiment series h09nz_ versus the tree data in the i09nz_ series would be created as follows:

```
h09nz1 01 12 1
h09nz2 01 12 1
h09nz3 01 12 1
h09nz4 01 12 1
h09nz5 01 12 1
h09nz6 01 12 1
h09nz7 01 12 1
h09nz8 01 12 1
h09nz9 01 12 1
h09nza 01 12 1
h09nzb 01 12 1
h09nzc 01 12 1
h09nzd 01 12 1

i09nz1 11 46 2
i09nz2 11 46 2
i09nz3 11 46 2
i09nz4 11 46 2
i09nz5 11 46 2
```

```
i09nz6 11 46 2
i09nz7 11 46 2
i09nz8 11 46 2
i09nz9 11 46 2
i09nza 11 46 2
i09nzb 11 46 2
i09nzc 11 46 2
i09nzd 11 46 2
```

The run-time for file d06nz_RUN1.m is about $3\frac{1}{2}$ hours on a SPARCstation 20. Therefore, all the variables, matrices, etc. calculated during the program run are saved as a .mat file. When the two files are re-named and modified to examine different targets and backgrounds in other data sets, the name of this output file should be made to relate to its contents. The current naming convention implemented in the program is the experiment series name followed by the frst data index of the target and background. The output file produced by d06nz_RUN1.m is therefore d06nz_00_68.mat.

multaccess and **access**

The command *multaccess* produces two-dimensional "wavelength-maps" of the data calculated and stored in an output file such as d06nz_00_68.mat, which was described above. The user must select which experiment to view. When this is done, multaccess.m produces the intensity maps of the five parameters SCR, R, G, and target and background ρ over the 2D wavelength space, and calls the command *access*. The file access.m begins a point-and click interface for retrieving parameter values from the data when a pair of wavelengths is selected by clicking with the mouse inside the axes of the figures. The first mouse button selects a point, the second cycles through the figures, and the third exits this process and returns the user to the MATLAB command line. This routine was designed for MATLAB running in Openwindows on a SPARCstation, and these routines will therefore most likely fail to run properly in a PC-based MATLAB environment. The screen output seen when using this command in MATLAB is provided below, along with two of the parameter maps which are produced:

```
>> load d06nz_00_68
>> multaccess

experiments =

d06nz1 d06nz2 d06nz3 d06nz4 d06nz5


Enter name of experiment to view results==> d06nz3

Warning: Log of zero
```

```
Warning: Divide by zero

Warning: Log of zero

Warning: Divide by zero
>>
```

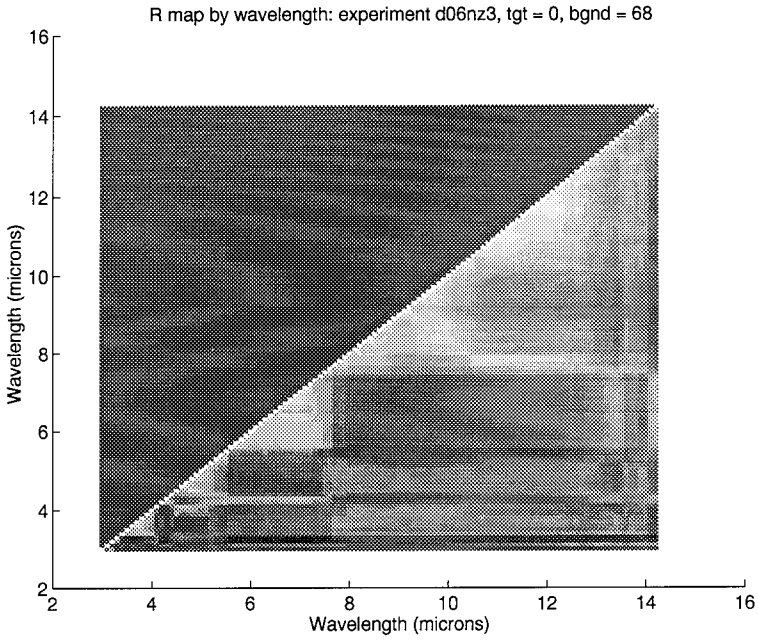

Figure 24. R Map Produced by command *multaccess*

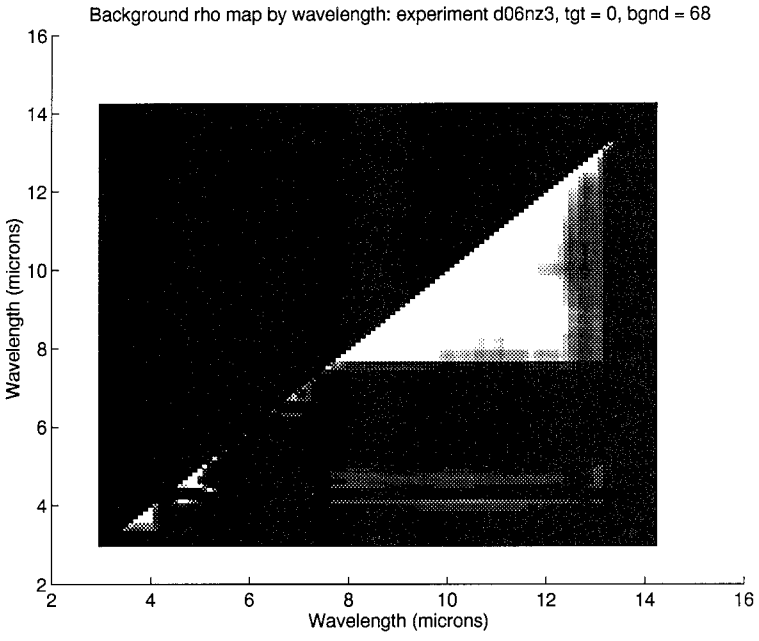

Figure 25. Background ρ Map produced by command *multaccess*

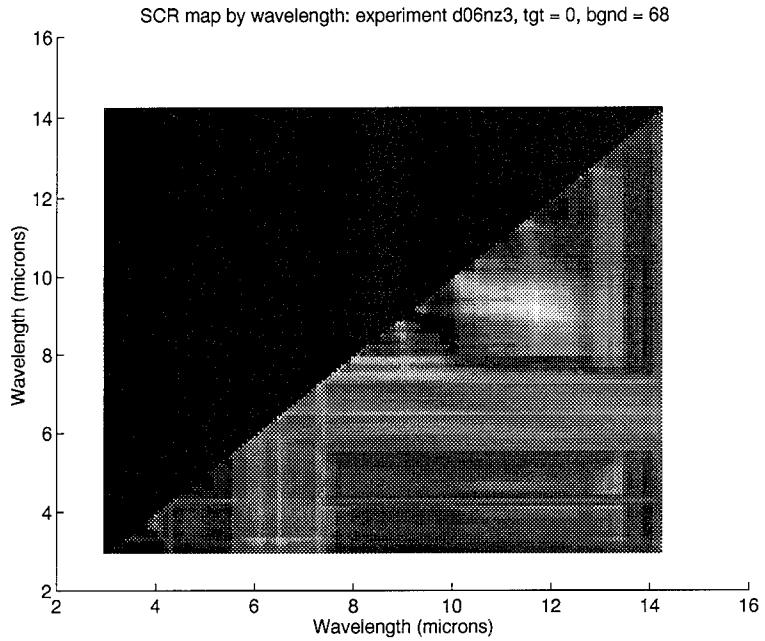

Figure 26. SCR Map produced by command *multaccess*

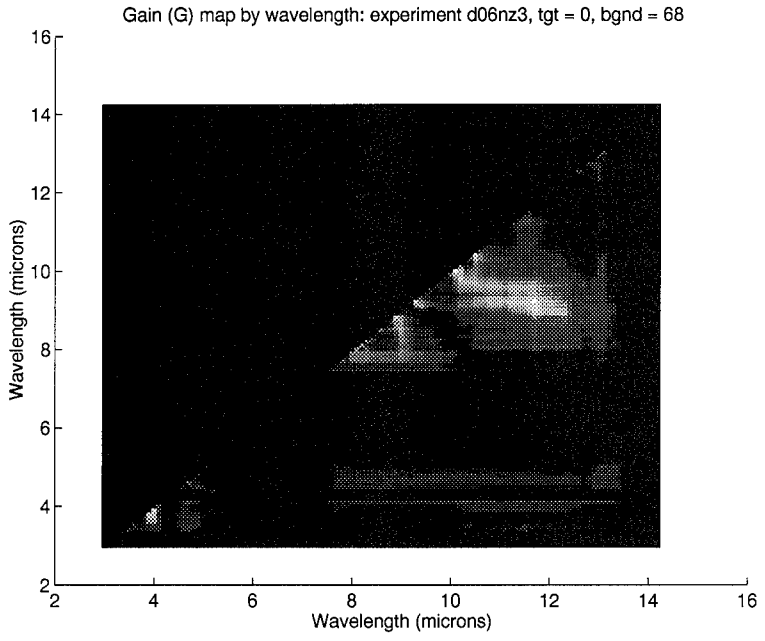

Figure 27. Multispectral Gain (G) Map produced by command *multaccess*

The command *access* may be invoked from the MATLAB command line to re-gain "access" to the current graphs if the user exits this interface, but then wishes to enter it again with the same figures without re-producing them with *multaccess*. Clicking on a portion of the SCR map with the 1st (left) mouse button gives the dual-band SCR at that wavelength pair for the target and background, as well as the color coefficient and background correlation. The m-file access.m also scatterplots the data at the chosen wavelengths in a sixth figure, and shows the results of detecting the targets by weighted-band differencing in a seventh. The two commands called by this m-file to perform these functions are, resectively, *rsp* and *suppress*. Examples of these plots for a selected wavelength pair from the maps of Figures 24–27 are given in Figures 28 and 29.

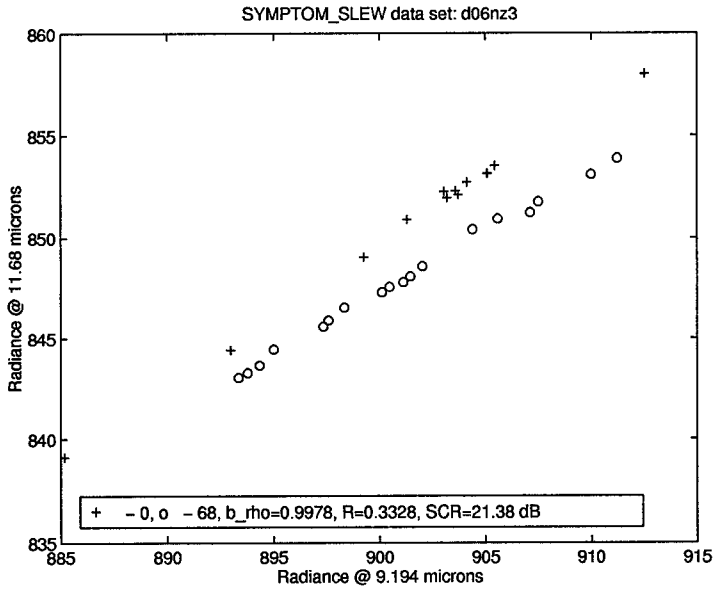

Figure 28. Scatterplot produced by command *rsp*

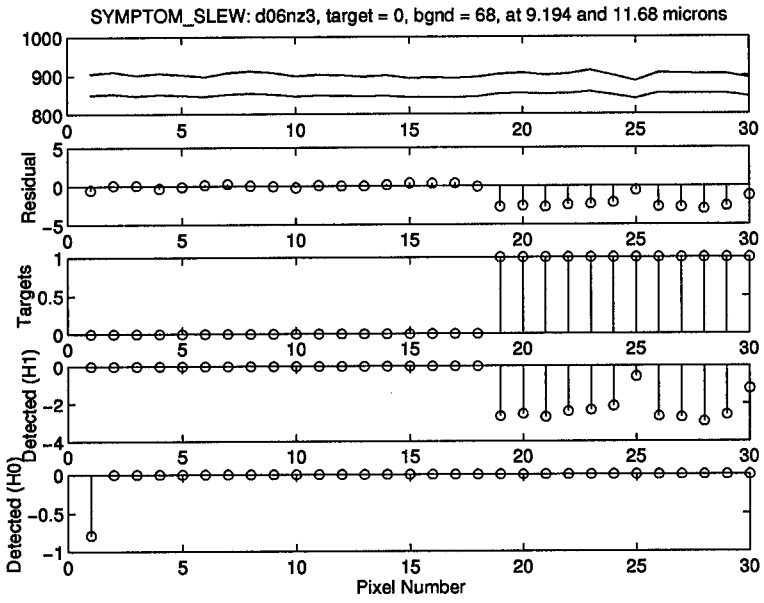

Figure 29. Weighted-Band Differencing Detection performed by command *suppress*

pairstats

This command is used to determine some of the statistics of several multispectral paramenters, such as *rho* and R for the various regions of the IR spectrum. The m-file which executes this command calls the subsidiary file bestbySCR_no_brho.m which ranks the bandpairs by dual-band SCR only, without regard to any other parameter (such as the background correlation). The ouput is a text file with '_pairstats' appended to a shortened name of the loaded .mat data file. For example, the output file for this command when used on the data in d06nz_00_68.mat is named d06_00_68_pairstats.

Portions of this output file are reproduced below:

(*Output of* d06_00_68_pairstats)

```
d06_00_68 d06nz1

 SCR          R        bgnd rho    tgtrho       G      wavelength_1  wavelength_2
27.06       0.7234      0.9639      0.9927     1.348       3.7          3.6
26.56       0.9743      0.9993      0.9999     1.205       8.4          8.3
26.29       0.9616      0.9982      0.9995     1.17        8.3          8.2
26.21       0.9664      0.9985      0.9999     1.165       8.6          8.5
26.16       0.7933      0.2685      0.9008     1.139       13.6         9.1
26.09       0.9689      0.9986      0.9997     1.146       8.8          8.5
26.08       0.9786      0.9996      1          1.251       11.9         11.8
26.08       0.8099      0.2569      0.9013     1.152       13.6         9.2
26.07       0.7962      0.2926      0.8991     1.13        13.6         8.3
26.06       0.799       0.2877      0.9009     1.134       13.6         9

percent of top 100 in MW = 1
percent of top 100 in LW = 90
percent of top 100 in MW/LW = 9
percent of top 100 w/ R<=0.2 = 0
percent of top 100 w/ brho>=0.99 = 15
```

percent of MW pairs w/ brho>=0.99 = 14.21
percent of LW pairs w/ brho>=0.99 = 24.63
percent of MW/LW pairs w/ brho>=0.99 = 0
percent of MW pairs w/ SCR>=18 dB and bro>=0.99 = 2.105
percent of LW pairs w/ SCR>=18 dB and bro>=0.99 = 21.4
percent of MW/LW pairs w/ SCR>=18 dB and bro>=0.99 = 0
percent of all 3403 bandpairs w/ SCR>=18.0 dB = 98.71
percent of all good pairs (SCRs>=18 dB) in MW = 5.418
percent of all good pairs (SCRs>=18 dB) in LW = 57.81
percent of all good pairs (SCRs>=18 dB) in MW/LW = 36.77
percent of all good pairs (SCRs>=18 dB) w/ R<=0.2 = 8.634
percent of all good pairs (SCRs>=18 dB) w/ brho>=0.99 = 12.56
percent of all good pairs (SCRs>=18 dB) w/ brho>=0.99 and R<=0.2 = 0

d06_00_68 d06nz2

SCR	R	bgnd rho	tgtrho	G	wavelength_1	wavelength_2
21	0.5049	0.9961	0.9975	5.651	11.3	9.2
20.71	0.4593	0.9946	0.9973	5.251	11.6	9.2
20.68	0.5194	0.9961	0.9977	5.527	11.2	9.2
20.68	0.4123	0.9933	0.9968	5.119	11.7	9.2

.
.
.

d06_00_68 d06nz5

SCR	R	bgnd rho	tgtrho	G	wavelength_1	wavelength_2
33.42	0.9685	0.9999	0.9999	2.991	10.2	9.8
32.96	0.9489	0.9998	0.9998	2.809	10.5	9.8
32.65	0.9503	0.9998	1	2.75	10.5	9.7
32.48	0.9571	0.9999	0.9999	2.667	10.4	9.8

.
.
.

d06_00_68 overall

SCR	R	bgnd rho	tgtrho	G	wavelength_1	wavelength_2
24.84	0.8158	0.9987	0.9998	4.157	10.5	9.7
24.69	0.7735	0.9974	0.9997	3.93	10.8	9.6
24.61	0.7294	0.996	0.9987	4.139	11.3	9.2

24.58	0.7389	0.9966	0.9988	4.119	11.2	9.2
24.57	0.6922	0.9946	0.9985	4.155	11.7	9.2
24.54	0.7236	0.9954	0.9988	4.013	11.4	9.2
24.54	0.7059	0.9952	0.9987	4.068	11.6	9.2
24.53	0.7686	0.9972	0.9997	3.805	10.9	9.6
24.47	0.717	0.9954	0.9988	3.943	11.5	9.2
24.47	0.8748	0.9995	0.9998	4.207	10.2	9.8

percent of top 100 in MW = 0
percent of top 100 in LW = 100
percent of top 100 in MW/LW = 0
percent of top 100 w/ R<=0.2 = 0
percent of top 100 w/ brho>=0.99 = 99
percent of MW pairs w/ brho>=0.99 = 18.42
percent of LW pairs w/ brho>=0.99 = 37.43
percent of MW/LW pairs w/ brho>=0.99 = 0
percent of MW pairs w/ SCR>=18 dB and bro>=0.99 = 1.579
percent of LW pairs w/ SCR>=18 dB and bro>=0.99 = 20.94
percent of MW/LW pairs w/ SCR>=18 dB and bro>=0.99 = 0
percent of all 3403 bandpairs w/ SCR>=18.0 dB = 29.89
percent of all good pairs (SCRs>=18 dB) in MW = 3.638
percent of all good pairs (SCRs>=18 dB) in LW = 69.32
percent of all good pairs (SCRs>=18 dB) in MW/LW = 27.04
percent of all good pairs (SCRs>=18 dB) w/ R<=0.2 = 0
percent of all good pairs (SCRs>=18 dB) w/ brho>=0.99 = 40.51
percent of all good pairs (SCRs>=18 dB) w/ brho>=0.99 and R<=0.2 = 0

pairscores

Like pairstats.m, this m-file prompts the user for a .mat data file. The program then rank orders all bandpairs (typically, a few hundred) for which average SCR over all experiments is greater than or equal to 18 dB and average background correlation is greater than or equal to 0.99. The bandpairs which meet these requirements are ranked by dual-band SCR and the score defined in this thesis. The subsidiary file which accomplishes this ranking and which is satrted within pairscores.m is names bestpairs.m.

The output of pairscores.m is a textfile which is named by appending the string '_scoredprs' to a shortened name of the loaded .mat data file. For example, the output file for this command when used on the data in d06nz_00_68.mat is named d06_00_68_scoredprs.

This output file is reproduced below:

(*Output of* d06_00_68_scoredprs)

d06_00_68 Pair selection by SCR alone

Top 15 bandpairs of 412

wvlth_1	wvlth_2	mean SCR	R	bgndrho	tgtrho	G	Rank	Scored #
10.5	9.7	24.84	0.8158	0.9987	0.9998	4.157	1	39
10.8	9.6	24.69	0.7735	0.9974	0.9997	3.93	2	35
11.3	9.2	24.61	0.7294	0.996	0.9987	4.139	3	3
11.2	9.2	24.58	0.7389	0.9966	0.9988	4.119	4	8
11.7	9.2	24.57	0.6922	0.9946	0.9985	4.155	5	1
11.4	9.2	24.54	0.7236	0.9954	0.9988	4.013	6	6
11.6	9.2	24.54	0.7059	0.9952	0.9987	4.068	7	2
10.9	9.6	24.53	0.7686	0.9972	0.9997	3.805	8	41
11.5	9.2	24.47	0.717	0.9954	0.9988	3.943	9	7
10.2	9.8	24.47	0.8748	0.9995	0.9998	4.207	10	59

10.9	9.2	24.43	0.7472	0.9968	0.999	3.965	11	17
11	9.2	24.43	0.7483	0.9968	0.9989	3.972	12	16
11.3	9.3	24.42	0.7481	0.9967	0.9992	3.971	13	11
11.7	9.1	24.4	0.6899	0.9934	0.9987	3.981	14	5
11.7	9.3	24.4	0.7096	0.9954	0.999	3.945	15	4

wvlth_1	wvlth_2	mean SCR	sdev(dB)	SCR1	SCR2	SCR3	SCR4	SCR5
10.5	9.7	24.84	6.509	24.76	18.35	18.51	29.96	32.65
10.8	9.6	24.69	6.256	25.28	18.26	18.36	30.06	31.47
11.3	9.2	24.61	4.128	25.3	21	19.74	27.93	29.07
11.2	9.2	24.58	4.367	25.34	20.68	19.47	28.18	29.21
11.7	9.2	24.57	3.455	25.37	20.68	21.38	26.72	28.72
11.4	9.2	24.54	4.289	25.34	20.32	19.89	27.86	29.28
11.6	9.2	24.54	3.777	25.3	20.71	20.57	27.18	28.92
10.9	9.6	24.53	6.233	25.52	17.95	18.24	29.7	31.22
11.5	9.2	24.47	4.251	25.34	20.36	19.78	27.63	29.23
10.2	9.8	24.47	6.783	24.97	17.57	18.05	28.33	33.42
10.9	9.2	24.43	4.986	25.35	19.73	18.8	28.65	29.62
11	9.2	24.43	4.926	25.28	19.75	18.9	28.67	29.52
11.3	9.3	24.42	4.697	25.36	20.45	18.7	28.36	29.25
11.7	9.1	24.4	4.072	25.64	19.22	21.16	27.1	28.89
11.7	9.3	24.4	4.062	25.42	20.01	20.33	27.27	28.97

Bottom 5 bandpairs of 412

wvlth_1	wvlth_2	mean SCR	R	bgndrho	tgtrho	G	Rank	Scored #
11.4	10.9	18.05	0.9569	0.9989	0.9999	1.584	946	408
11.4	10.8	18.04	0.9493	0.9986	0.9999	1.581	953	409
11.3	11.1	18.03	0.9608	0.9995	0.9999	1.62	961	410
10.9	10.5	18.01	0.9341	0.9986	0.9998	1.729	1000	411
11.4	10.6	18	0.9254	0.9973	0.9998	1.55	1012	412

wvlth_1	wvlth_2	mean SCR	sdev(dB)	SCR1	SCR2	SCR3	SCR4	SCR5
11.4	10.9	18.05	8.608	24.58	8.468	9.036	22.05	26.09
11.4	10.8	18.04	8.398	24.87	8.676	9.303	21.68	25.67
11.3	11.1	18.03	8.858	25.07	10.34	6.851	21.72	26.18
10.9	10.5	18.01	8.781	25.64	8.544	8.587	21.61	25.69
11.4	10.6	18	8.633	25.07	8.703	8.644	21.95	25.65

d06_00_68 Pair selection by score

Top 15 bandpairs of 412

wvlth_1	wvlth_2	Score	mean SCR	R	bgndrho	tgtrho	G	Rank
11.7	9.2	1.903	24.57	0.6922	0.9946	0.9985	4.155	5
11.6	9.2	1.731	24.54	0.7059	0.9952	0.9987	4.068	7
11.3	9.2	1.601	24.61	0.7294	0.996	0.9987	4.139	3
11.7	9.3	1.576	24.4	0.7096	0.9954	0.999	3.945	15
11.7	9.1	1.572	24.4	0.6899	0.9934	0.9987	3.981	14
11.4	9.2	1.524	24.54	0.7236	0.9954	0.9988	4.013	6
11.5	9.2	1.522	24.47	0.717	0.9954	0.9988	3.943	9
11.2	9.2	1.506	24.58	0.7389	0.9966	0.9988	4.119	4
11.6	9.3	1.464	24.36	0.7239	0.996	0.9992	3.885	16
11.8	9.2	1.462	24.15	0.7017	0.9939	0.9984	3.748	28
11.3	9.3	1.367	24.42	0.7481	0.9967	0.9992	3.971	13
11.6	9.1	1.356	24.13	0.7036	0.9938	0.9989	3.733	31
11.7	9	1.338	24.27	0.7031	0.9935	0.999	3.898	22
11.5	9.3	1.31	24.27	0.7346	0.9962	0.9992	3.785	21
11.4	9.3	1.309	24.33	0.7418	0.9962	0.9993	3.845	19

wvlth_1	wvlth_2	mean SCR	sdev(dB)	SCR1	SCR2	SCR3	SCR4	SCR5
11.7	9.2	24.57	3.455	25.37	20.68	21.38	26.72	28.72
11.6	9.2	24.54	3.777	25.3	20.71	20.57	27.18	28.92
11.3	9.2	24.61	4.128	25.3	21	19.74	27.93	29.07
11.7	9.3	24.4	4.062	25.42	20.01	20.33	27.27	28.97
11.7	9.1	24.4	4.072	25.64	19.22	21.16	27.1	28.89
11.4	9.2	24.54	4.289	25.34	20.32	19.89	27.86	29.28
11.5	9.2	24.47	4.251	25.34	20.36	19.78	27.63	29.23
11.2	9.2	24.58	4.367	25.34	20.68	19.47	28.18	29.21
11.6	9.3	24.36	4.347	25.36	20.12	19.55	27.69	29.1
11.8	9.2	24.15	4.207	25.22	19.62	19.85	27.54	28.52
11.3	9.3	24.42	4.697	25.36	20.45	18.7	28.36	29.25
11.6	9.1	24.13	4.518	25.55	18.92	19.82	27.41	28.94
11.7	9	24.27	4.684	25.55	18.04	20.89	27.63	29.23
11.5	9.3	24.27	4.788	25.43	19.79	18.77	28.02	29.37
11.4	9.3	24.33	4.83	25.39	19.66	18.92	28.23	29.43

Bottom 5 bandpairs of 412

wvlth_1	wvlth_2	Score	mean SCR	R	bgndrho	tgtrho	G	Rank
11.4	10.9	0.005235	18.05	0.9569	0.9989	0.9999	1.584	946
11.4	10.8	0.004727	18.04	0.9493	0.9986	0.9999	1.581	953
11.3	11.1	0.003944	18.03	0.9608	0.9995	0.9999	1.62	961
10.9	10.5	0.00141	18.01	0.9341	0.9986	0.9998	1.729	1000
11.4	10.6	0.0004795	18	0.9254	0.9973	0.9998	1.55	1012

wvlth_1	wvlth_2	mean SCR	sdev(dB)	SCR1	SCR2	SCR3	SCR4	SCR5
11.4	10.9	18.05	8.608	24.58	8.468	9.036	22.05	26.09
11.4	10.8	18.04	8.398	24.87	8.676	9.303	21.68	25.67
11.3	11.1	18.03	8.858	25.07	10.34	6.851	21.72	26.18
10.9	10.5	18.01	8.781	25.64	8.544	8.587	21.61	25.69
11.4	10.6	18	8.633	25.07	8.703	8.644	21.95	25.65

d06_00_68 Performance comparison

		SCR1	SCR2	SCR3	SCR4	SCR5
means in dB, first 10 SCRs		25.25	19.59	19.4	28.36	30.32
means in dB, first 10 scores		25.36	20.27	20.17	27.51	28.99
means in dB, first 15 SCRs		25.3	19.67	19.46	28.24	29.96
means in dB, first 15 scores		25.39	19.97	19.92	27.65	29.07
means in dB, first 50 SCRs		25.28	18.64	18.64	28.39	30.06
means in dB, first 50 scores		25.36	18.69	18.94	28.05	29.42
location of highest mean	(SCRs)	0	0	0	1	1
	(scores)	1	1	1	0	0
	(SCRs)	0	0	0	1	1
	(scores)	1	1	1	0	0
	(SCRs)	0	0	0	1	1
	(scores)	1	1	1	0	0
minimums in dB, first 10 SCRs		24.76	17.57	18.05	26.72	28.72
minimums in dB, first 10 scores		25.22	19.22	19.47	26.72	28.52

minimums in dB, first 15 SCRs		24.76	17.57	18.05	26.72	28.72
minimums in dB, first 15 scores		25.22	18.04	18.7	26.72	28.52
minimums in dB, first 50 SCRs		24.74	16.71	16.86	26.72	28.52
minimums in dB, first 50 scores		24.76	16.8	17.42	26.65	28.15
location of minimum	(SCRs)	1	1	1	0	0
	(scores)	0	0	0	0	1
	(SCRs)	1	1	1	0	0
	(scores)	0	0	0	0	1
	(SCRs)	1	1	1	0	0
	(scores)	0	0	0	1	1
maximums in dB, first 10 SCRs		25.52	21	21.38	30.06	33.42
maximums in dB, first 10 scores		25.64	21	21.38	28.18	29.28
maximums in dB, first 15 SCRs		25.64	21	21.38	30.06	33.42
maximums in dB, first 15 scores		25.64	21	21.38	28.36	29.43
maximums in dB, first 50 SCRs		25.64	21	21.38	30.06	33.42
maximums in dB, first 50 scores		25.8	21	21.38	30.06	32.65
location of maximum	(SCRs)	0	0	0	1	1
	(scores)	1	0	0	0	0
	(SCRs)	0	0	0	1	1
	(scores)	0	0	0	0	0
	(SCRs)	0	0	0	0	1
	(scores)	1	0	0	0	0

d06_00_68 Pair selection by SCR alone MW pairs only

Top 3 MW bandpairs of 3

wvlth_1	wvlth_2	mean SCR	R	bgndrho	tgtrho	G	SCR #	Scored #
4.9	4.5	18.46	0.8338	0.9965	0.9987	2.671	365	373

5	4.5	18.29	0.7496	0.9914	0.9938	2.439	381	382
5.1	5	18.15	0.785	0.9904	0.972	1.911	394	391

wvlth_1	wvlth_2	mean SCR	sdev(dB)	SCR1	SCR2	SCR3	SCR4	SCR5
4.9	4.5	18.46	9.808	23.15	12.06	4.768	23.35	28.97
5	4.5	18.29	8.384	24.14	15.76	5.249	19.72	26.56
5.1	5	18.15	8.233	24.59	15.07	5.572	19.61	25.89

d06_00_68 Pair selection by score MW pairs only

Top 3 MW bandpairs of 3

wvlth_1	wvlth_2	Score	mean SCR	R	bgndrho	tgtrho	G	Score Rank
4.9	4.5	0.04698	18.46	0.8338	0.9965	0.9987	2.671	373
5	4.5	0.03419	18.29	0.7496	0.9914	0.9938	2.439	382
5.1	5	0.01773	18.15	0.785	0.9904	0.972	1.911	391

wvlth_1	wvlth_2	mean SCR	sdev(dB)	SCR1	SCR2	SCR3	SCR4	SCR5
4.9	4.5	18.46	9.808	23.15	12.06	4.768	23.35	28.97
5	4.5	18.29	8.384	24.14	15.76	5.249	19.72	26.56
5.1	5	18.15	8.233	24.59	15.07	5.572	19.61	25.89

finalpairs

The finalpairs.m program looks at a number of experiment series (several .mat data files) at once. It identifies the bandpairs which meet the criteria set forth in the section on command *scoredpairs* for each series. The purpose is to use data from several days to produce a final rank-ordered list of bandpairs which display the 'best' multispectral detection performance. Once again, the two choices for evaluating this property of the bandpairs, are ranking by highest average SCR, and highest total score. This program then uses the m-file finaldet.m to look at the multipectral target and bachground data and attempt detection of the target pixels for a specified number of the top-ranked bandpairs. This is done for the SCR- and score-ranked bandpairs and comparison is made based upon the numbers of pixels correctly detected and the number falsely determined to be targets under both H_1 and H_0 conditions. The results of this comparison are printed to a text file with the prefix 'finaldet'. The current m-file examines the data files d0(6,7,8)nz_00_68, and places output in the file 'finaldet_M752_10', defined in the code itself. The '_10' indicates that comparison between the ranking methods was performed for the top 10 bandpairs.

In addition, finaldet.m creates an ouput text file of its own and places information about the final bandpair lists for both selection by SCR and by score. The file divides the output into bandpairs which are common to both lists and those which are unique to each. The naming convention for this output file is some form of the first .mat filename and a prefix of 'finalpairs'.

Examples of these output files are provided.

finalpairs

The finalpairs.m program looks at a number of experiment series (several .mat data files) at once. It identifies the bandpairs which meet the criteria set forth in the section on command *scoredpairs* for each series. The purpose is to use data from several days to produce a final rank-ordered list of bandpairs which display the 'best' multispectral detection performance. Once again, the two choices for evaluating this property of the bandpairs, are ranking by highest average SCR, and highest total score. This program then uses the m-file finaldet.m to look at the multipectral target and bachground data and attempt detection of the target pixels for a specified number of the top-ranked bandpairs. This is done for the SCR- and score-ranked bandpairs and comparison is made based upon the numbers of pixels correctly detected and the number falsely determined to be targets under both H_1 and H_0 conditions. The results of this comparison are printed to a text file with the prefix 'finaldet'. The current m-file examines the data files d0(6,7,8)nz_00_68, and places output in the file 'finaldet_M752_10', defined in the code itself. The '_10' indicates that comparison between the ranking methods was performed for the top 10 bandpairs.

In addition, finaldet.m creates an ouput text file of its own and places information about the final bandpair lists for both selection by SCR and by score. The file divides the output into bandpairs which are common to both lists and those which are unique to each. The naming convention for this output file is some form of the first .mat filename and a prefix of 'finalpairs'.

Examples of these output files are provided.

(*Output of* finalpairsd06_00_68)

M752 Lance (listsize 10) and Tree Canopy dissimilar final pair selection by SCR

position	wl_1	wl_2	SCR
7	10.8	9.2	23.36
9	11.9	9.2	23.33
10	11	9.2	23.33

M752 Lance (listsize 10) and Tree Canopy dissimilar final pair selection by score

position	wl_1	wl_2	score
8	11.6	9.3	1.135
9	11.8	9.3	1.115
10	11.5	9.3	1.105

M752 Lance (listsize 10) and Tree Canopy Common final pair selection

SCR pos.	wl_1	wl_2	SCR	score pos.	wl_1	wl_2	score
1	11.6	9.2	23.52	1	11.6	9.2	1.207
2	11.8	9.2	23.5	4	11.8	9.2	1.162
3	11.5	9.2	23.46	2	11.5	9.2	1.176
4	11.4	9.2	23.44	5	11.4	9.2	1.155
5	11.2	9.2	23.38	7	11.2	9.2	1.148
6	11.7	9.2	23.37	3	11.7	9.2	1.174
8	11.3	9.2	23.34	6	11.3	9.2	1.154

(*Output of* finaldet_M752_10)

M752 Lance (listsize 10) and trees for d06nz1

SCRwins	scorewins	ties
2	0	8

M752 Lance (listsize 10) and trees for d06nz2

SCRwins	scorewins	ties
3	2	5

M752 Lance (listsize 10) and trees for d06nz3

SCRwins	scorewins	ties
0	2	8

M752 Lance (listsize 10) and trees for d06nz4

SCRwins	scorewins	ties
0	0	10

M752 Lance (listsize 10) and trees for d06nz5

SCRwins	scorewins	ties
4	2	4

M752 Lance (listsize 10) and trees for d07nz1

SCRwins	scorewins	ties
5	3	2

M752 Lance (listsize 10) and trees for d07nz2

SCRwins	scorewins	ties
2	1	7

M752 Lance (listsize 10) and trees for d07nz3

SCRwins	scorewins	ties
2	1	7

M752 Lance (listsize 10) and trees for d07nz4

SCRwins	scorewins	ties
0	0	10

M752 Lance (listsize 10) and trees for d07nz5

SCRwins	scorewins	ties
0	0	10

M752 Lance (listsize 10) and trees for d08nz1

SCRwins	scorewins	ties
4	5	1

M752 Lance (listsize 10) and trees for d08nz2

SCRwins	scorewins	ties
2	7	1

M752 Lance (listsize 10) and trees for d08nz3

SCRwins	scorewins	ties
2	2	6

M752 Lance (listsize 10) and trees for d08nz4

SCRwins	scorewins	ties
0	0	10

M752 Lance (listsize 10) and trees for d08nz5

SCRwins	scorewins	ties
2	0	8

Bibliography

1. Cederquist, J., et al., "Infrared Multispectral Sensor Program, Phase 2: Field Measurments, Analysis and Modeling." Prepared for Wright Laboratory/AARI-4, WPAFB, OH under Contract F33615-90-C-1441, October 1993. Vol. 2: Redstone Arsenal Measurements Catalog.
2. Cederquist, J., et al., "Infrared Multispectral Sensor Program, Phase 2: Field Measurments, Analysis and Modeling." Prepared for Wright Laboratory/AARI-4, WPAFB, OH under Contract F33615-90-C-1441, May 1994. Vol. 1: Fourier Transform Spectrometer Sensor Characterization.
3. Chen, J. and I. Reed. "A Detection Algorithm for Optical Targets in Clutter," *IEEE Trans. on Aerospace and Electronic Systems, AES-23*(1) (Jan 1987).
4. Hardie, Russel C., "Adaptive Quadratic Classifiers for Multispectral Target Detection." Final report for Summer Faculty Research Program, Wright Laboratory, August 1994.
5. Hunt, B. R. and T. M. Cannon. "Non-stationary Assumptions of Gaussian Models of Images," *IEEE Trans. on Systems, Man and Cybernetics* (Dec 1976).
6. Johnson, R. and D. Wichern. *Applied Multivariate Statistical Analysis.* Englewood Cliffs, New Jersey: Prentice-Hall, Inc., 1982.
7. Johnson, R. O. Capt., USAF. Wright Laboratory. Personal Interviews. Wright Laboratory, Wright-Patterson AFB, Ohio. 10 Jun - 26 Sep 1994.
8. Mannos, J. and D. Sakrison. "The Effects of a Visual Fidelity Crierion on the Encoding of Images," *IEEE Trans. on Information Theory, IT-20*:525–536 (July 1974).
9. Margalit, A., et al. "Adaptive Optical Detection Using Correlated Images," *IEEE Trans. on Aerospace and Electronic Systems, AES-21*(3) (May 1985).
10. Pratt, William K. *Digital Image Processing.* New York: John Wiley and Sons Inc., 1978.
11. Schalkoff, R. *Pattern Recognition: Statistical, Structural and Neural Approaches.* New York: John Wiley and Sons, Inc., 1992.
12. Seyrafi, Khalil. *Electro-Optical Systems Analysis.* Los Angeles, CA: Electro-Optical Research Company, 1985.
13. Stocker, A., et al. "Analysis of Infrared Multi-Spectral Target/Background Field Measurements," *Proceedings from the SPIE International Symposium on Optical Engineering in Aerospace Sensing, Orlando, FL* (April 1994).
14. Stocker, A., et al. "Multi-dimensional Signal Processing for Electro-optical Target Detection," *SPIE Vol. 1305 Signal and Data Processing of Small Targets* (April 1990).
15. Stocker, A., et al. "Adaptive Detection of Sub-Pixel Targets Using Multi-Band Frame Sequences," *SPIE Vol. 1481 Signal and Data Processing of Small Targets* (January 1991).

16. Stotts, L. B., et al. "Clutter Rejection Using Multi-spectral Processing," *SPIE Vol. 1305 Signal and Data Processing of Small Targets* (October 1990).

17. Thomas, John B. *Introduction to Probability*. New York: Springer-Verlag, 1986.

18. Yu, X., et al. "Comparative Performance Analysis of Multispectral Detectors," *IEEE Trans. on Signal Processing*, *41*(8) (Aug 1993).

Vita

Lieutenant Jason E. Thomas was born May 31, 1971 in Oklahoma City, Oklahoma to Ray and Susan Thomas of Norman. Soon thereafter, his family was forced to spend several years in Texas, as his father was, at that time, a U.S. Air Force officer. The family later returned to Norman where Lt. Thomas remained until graduating from Norman High School in May 1989, and entering the U.S. Air force Academy at Colorado springs, CO that June. Four years later on June 2, 1993 he found himself with a commission and graduate degree in Electrical Engineering as a member of the Academy's 35th graduating class. His first assignment was to earn the MS degree in Electrical Engineeering at the Air Force Institute of Technology where, in 1994, he became engaged to the gracious and lovely Miss Suzanne E. Fitch of Colorado Springs.

Permanent address: 2501 Acacia Ct.
Norman, Oklahoma 73072

REPORT DOCUMENTATION PAGE

Form Approved
OMB No. 0704-0188

1. AGENCY USE ONLY (Leave blank)	2. REPORT DATE	3. REPORT TYPE AND DATES COVERED
	December 1994	Master's Thesis

4. TITLE AND SUBTITLE

Multispectral Detection of Ground Targets in Highly Correlated Backgrounds

5. FUNDING NUMBERS

6. AUTHOR(S)

Jason E Thomas

7. PERFORMING ORGANIZATION NAME(S) AND ADDRESS(ES)

Air Force Institute of Technology
WPAFB OH 45433-6583

8. PERFORMING ORGANIZATION REPORT NUMBER

AFIT/GEO/ENP/94D-06

9. SPONSORING / MONITORING AGENCY NAME(S) AND ADDRESS(ES)

CAPT Ray O. Johnson
WL/AARI, WPAFB OH 45433-7408

10. SPONSORING / MONITORING AGENCY REPORT NUMBER

11. SUPPLEMENTARY NOTES

12a. DISTRIBUTION / AVAILABILITY STATEMENT

Approved for Public Release;Distribution Unlimited

12b. DISTRIBUTION CODE

Multispectral detection methods attempt to discriminate targets in a dominant clutter background using multiple images of the same real-world scene taken in different narrow spectral bands in the infrared. Detection is possible due to the empirically-observed phenomenon that the radiance of man-made objects, such as a tank or truck, often lies off the main spectral correlation axis of that of natural backgrounds. Radiometric measurements of several vehicles and a tree canopy background taken over three days in June, 1994 were used to examine the factors affecting multispectral detection. Results clearly showed that the processes which provide for higher spectral correlation of natural backgrounds tend to diminish the spectral separation between the background and target. Very high correlations between IR spectral bands for the targets and background were found to exist. The degree of correlation between bands in the LWIR was found to be higher than that for the MWIR for the correlation levels (ρ) of interest, $\rho \geq 0.99$. The MW/LW combinations were found to almost never produce these high correlations. In addition, a scoring method for use in ranking pairs of spectral band pairs over multiple collection instances was developed and evaluated. The score was intended to rank combinations of spectral bands which provide consistent, if moderate, performance over bands which may provide both excellent and unacceptable signal-to-clutter ratios (SCRs) over the same observation period. The scoring method found more stable spectral pairs, and, for data reflecting more difficult detection situations, produced rank-ordered lists of wavelength pairs which exhibited higher mean, minimum, and maximum SCRs than were produced by simply ranking the bandpairs by average SCR value.

14. SUBJECT TERMS

Multispectral, Hyperspectral, Infrared, Covariance, Correlation, Gaussian, Multivariate Distribution, Random Variable, Matched Filter, 'RX' Filter, Dual-Band Signal-to-Clutter Ratio, Dual-Band Gain

15. NUMBER OF PAGES

112

17. SECURITY CLASSIFICATION OF REPORT	18. SECURITY CLASSIFICATION OF THIS PAGE	19. SECURITY CLASSIFICATION OF ABSTRACT	20. LIMITATION OF ABSTRACT
UNCLASSIFIED	UNCLASSIFIED	UNCLASSIFIED	UL